

Implementation of a Precast Inverted T-Beam System in Virginia: Part I: Laboratory Investigations

http://www.virginiadot.org/vtrc/main/online_reports/pdf/18-r7.pdf

FATMIR MENKULASI, Ph.D., P.E.
Assistant Professor
Department of Civil and Environmental Engineering
Wayne State University

THOMAS E. COUSINS, Ph.D., P.E.
Professor
Glenn Department of Civil Engineering
Clemson University

CARIN L. ROBERTS-WOLLMANN, Ph.D., P.E.
Professor
Via Department of Civil and Environmental Engineering
Virginia Tech

Via Department of Civil and Environmental Engineering
Virginia Polytechnic Institute and State University

Final Report VTRC 18-R7

Standard Title Page - Report on Federally Funded Project

1. Report No.: FHWA/VTRC 18-R7	2. Government Accession No.:	3. Recipient's Catalog No.:	
4. Title and Subtitle: Implementation of a Precast Inverted T-Beam System in Virginia: Part I: Laboratory Investigations		5. Report Date: October 2017	
		6. Performing Organization Code:	
7. Author(s): Fatmir Menkulasi, Ph.D., P.E., Thomas E. Cousins, Ph.D., P.E., and Carin L. Roberts-Wollmann, Ph.D., P.E.		8. Performing Organization Report No.: VTRC 18-R7	
9. Performing Organization and Address The Charles E. Via, Jr. Department of Civil and Environmental Engineering Virginia Polytechnic Institute and State University Blacksburg, VA		10. Work Unit No. (TRAIS):	
		11. Contract or Grant No.: 101740	
12. Sponsoring Agencies' Name and Address: Virginia Department of Transportation Federal Highway Administration 1401 E. Broad Street 400 North 8th Street, Room 750 Richmond, VA 23219 Richmond, VA 23219-4825		13. Type of Report and Period Covered: Final Contract	
		14. Sponsoring Agency Code:	
15. Supplementary Notes:			
<p>16. Abstract:</p> <p>The inverted T-beam system provides an accelerated bridge construction alternative for short-to-medium-span bridges. The system consists of adjacent precast inverted T-beams with a cast-in-place concrete topping. This bridge system is not expected to experience the reflective cracking problems manifested in short-to-medium-span bridges constructed with the traditional adjacent voided slab or adjacent box beam systems. This report presents the results of three phases of a comprehensive research project to develop and implement an inverted T-beam system for Virginia. The three phases are shape and transverse connection design, cast-in-place topping optimization, and composite action.</p> <p>When concentrated loads are applied to a bridge of this type, the bridge deforms as a two-way flat plate. This phase of testing included an analytical and experimental investigation focused on the first inverted T-beam bridge in Virginia on US 360 over the Chickahominy River to study the relationship between transverse bending and reflective cracking. Transverse bending moment demands were quantified using a finite element model and compared to tested transverse bending moment capacities provided by several sub-assembly specimens. The tested sub-assembly specimens featured a combination of various precast inverted T-beam cross-sectional shapes and transverse connections. It was concluded that all tested specimens performed well at service load levels. The detail that features a precast inverted T-beam with tapered webs and no mechanical connection between the adjacent inverted T-beams and cast-in-place topping is the simplest and most economical.</p> <p>There is a difference in shrinkage properties between the inverted T-beam and the deck because of the sequence of construction. The deck is subject to restrained shrinkage tensile stresses, which may lead to cracking. This phase of testing included an experimental study on the short-term and long-term properties of seven deck mixtures to identify a deck mixture with low shrinkage and high creep. The mixture with saturated lightweight fine aggregates is expected to best alleviate tensile stresses due to differential shrinkage.</p> <p>The final phase of testing presented in this report investigated the composite action between the unique precast and cast-in-place element shapes. A full-scale composite beam was tested under different loading arrangements with the purpose of simulating the service level design moment, strength level design shear, strength level design moment and nominal flexural strength. To investigate the necessity of extended stirrups, half of the span featured extended stirrups, whereas the other half featured no extended stirrups. In the tests, the system behaved compositely at all loading levels and no slip occurred at the interface. In addition to measuring slip at various interface locations, full composite action was verified by comparing load displacement curves obtained analytically and experimentally. It is concluded that because of the large contact surface between the precast and cast-in-place elements, cohesion alone appears to provide the necessary horizontal shear strength to ensure full composite action.</p>			
17 Key Words: Full-depth precast bridge deck panels, panel-to-panel connections, block-out surface treatments		18. Distribution Statement: No restrictions. This document is available to the public through NTIS, Springfield, VA 22161.	
19. Security Classif. (of this report): Unclassified	20. Security Classif. (of this page): Unclassified	21. No. of Pages: 70	22. Price:

FINAL REPORT

**IMPLEMENTATION OF A PRECAST INVERTED T-BEAM SYSTEM
IN VIRGINIA: PART I: LABORATORY INVESTIGATIONS**

Fatmir Menkulasi, Ph.D., P.E.
Assistant Professor
Department of Civil and Environmental Engineering
Wayne State University

Thomas E. Cousins, Ph.D., P.E.
Professor
Glenn Department of Civil Engineering
Clemson University

Carin L. Roberts-Wollmann, Ph.D., P.E.
Professor
Via Department of Civil and Environmental Engineering
Virginia Tech

Via Department of Civil and Environmental Engineering
Virginia Polytechnic Institute and State University

Project Manager

Bernard L. Kassner, Ph.D., P.E., Virginia Transportation Research Council

Virginia Transportation Research Council
(A partnership of the Virginia Department of Transportation
And the University of Virginia since 1948)

Charlottesville, Virginia

October 2017
VTRC 18-R7

DISCLAIMER

The project that is the subject of this report was done under contract for the Virginia Department of Transportation, Virginia Transportation Research Council. The contents of this report reflect the views of the authors, who are responsible for the facts and the accuracy of the data presented herein. The contents do not necessarily reflect the official views or policies of the Virginia Department of Transportation, the Commonwealth Transportation Board, or the Federal Highway Administration. This report does not constitute a standard, specification, or regulation. Any inclusion of manufacturer names, trade names, or trademarks is for identification purposes only and is not to be considered an endorsement.

Each contract report is peer reviewed and accepted for publication by staff of Virginia Transportation Research Council with expertise in related technical areas. Final editing and proofreading of the report are performed by the contractor.

Copyright 2017 by the Commonwealth of Virginia.
All rights reserved.

ABSTRACT

The inverted T-beam system provides an accelerated bridge construction alternative for short-to-medium-span bridges. The system consists of adjacent precast inverted T-beams with a cast-in-place concrete topping. This bridge system is not expected to experience the reflective cracking problems manifested in short-to-medium-span bridges constructed with the traditional adjacent voided slab or adjacent box beam systems. This report presents the results of three phases of a comprehensive research project to develop and implement an inverted T-beam system for Virginia. The three phases are shape and transverse connection design, cast-in-place topping optimization, and composite action.

When concentrated loads are applied to a bridge of this type, the bridge deforms as a two-way flat plate. This phase of testing included an analytical and experimental investigation focused on the first inverted T-beam bridge in Virginia on US 360 over the Chickahominy River to study the relationship between transverse bending and reflective cracking. Transverse bending moment demands were quantified using a finite element model and compared to tested transverse bending moment capacities provided by several sub-assembly specimens. The tested sub-assembly specimens featured a combination of various precast inverted T-beam cross-sectional shapes and transverse connections. It was concluded that all tested specimens performed well at service load levels. The detail that features a precast inverted T-beam with tapered webs and no mechanical connection between the adjacent inverted T-beams and cast-in-place topping is the simplest and most economical.

There is a difference in shrinkage properties between the inverted T-beam and the deck because of the sequence of construction. The deck is subject to restrained shrinkage tensile stresses, which may lead to cracking. This phase of testing included an experimental study on the short-term and long-term properties of seven deck mixtures to identify a deck mixture with low shrinkage and high creep. The mixture with saturated lightweight fine aggregates is expected to best alleviate tensile stresses due to differential shrinkage.

The final phase of testing presented in this report investigated the composite action between the unique precast and cast-in-place element shapes. A full-scale composite beam was tested under different loading arrangements with the purpose of simulating the service level design moment, strength level design shear, strength level design moment and nominal flexural strength. To investigate the necessity of extended stirrups, half of the span featured extended stirrups, whereas the other half featured no extended stirrups. In the tests, the system behaved compositely at all loading levels and no slip occurred at the interface. In addition to measuring slip at various interface locations, full composite action was verified by comparing load displacement curves obtained analytically and experimentally. It is concluded that because of the large contact surface between the precast and cast-in-place elements, cohesion alone appears to provide the necessary horizontal shear strength to ensure full composite action.

FINAL REPORT

IMPLEMENTATION OF A PRECAST INVERTED T-BEAM SYSTEM IN VIRGINIA: PART I: LABORATORY INVESTIGATIONS

Fatmir Menkulasi, Ph.D., P.E.
Assistant Professor
Department of Civil and Environmental Engineering
Wayne State University

Thomas E. Cousins, Ph.D., P.E.
Professor
Glenn Department of Civil Engineering
Clemson University

Carin L. Roberts-Wollmann, Ph.D., P.E.
Professor
Via Department of Civil and Environmental Engineering
Virginia Tech

Via Department of Civil and Environmental Engineering
Virginia Polytechnic Institute and State University

INTRODUCTION

Prefabricated Bridge Construction

Prefabricated bridge construction typically consists of fabricating individual elements off-site and delivering them to the project site ready to be erected. This allows the concurrent production of the individual elements, as opposed to cast-in-place concrete construction, in which the casting of a certain component can be done only if the supporting element is in place. The fabrication of elements off-site also eliminates the need to construct and remove formwork at the bridge site, work in close proximity to traffic, or operate in areas that are over water. The accelerated bridge construction offered by precast elements has been embraced by engineers and is being widely used in the United States.

Similar to structural steel building and bridge construction, the fabrication of a concrete bridge structure in individual pieces raises the question of how these components will be connected. In prefabricated bridge construction, it is typically these connections that deteriorate over time and create the need for bridge rehabilitation or replacement. It is in this area that cast-in-place concrete construction has an advantage over prefabricated construction because it reduces the number of joints, which are the problematic areas, and it offers a higher degree of redundancy, which in some cases is desirable. The challenge that engineers face today is how to design structures that consist of prefabricated elements but emulate the durability of monolithic construction.

FHWA Scanning Tour

The Federal Highway Administration (FHWA) and the American Association of State Highway and Transportation Officials (AASHTO) initiated a scanning tour in April 2004 to explore state-of-the-art technologies for rapid construction already being implemented in other industrialized countries (Ralls et al., 2005). A team of eleven members (three representatives from FHWA, four representatives from state departments of transportation, one representative from county engineers, one university representative, and two representatives from industry) visited Japan, the Netherlands, Belgium, Germany, and France with the objective to identify international uses of prefabricated bridge elements and systems and to identify decision processes, design methodologies, construction techniques, costs, and maintenance and inspection issues associated with use of the technology. The team was interested in all aspects of design, construction, and maintenance of bridge systems composed of multiple elements that are fabricated and assembled off-site.

One of the systems identified in the scanning tour for implementation in the United States was the Poutre-Dalle system (Figure 1). This system was observed in France and “poutre-dalle” in French means beam-slab. The system consists of a series of adjacent precast inverted T-beams that serve as formwork for the cast-in-place topping. After the cast-in-place topping is placed, the system behaves as a composite slab. It eliminates the need for installing formwork on site and provides a connection between the precast and cast-in-place components through the transverse hooked bars protruding from the webs of the precast inverted T-beam. The Poutre-Dalle system is intended for short-to-medium-span bridges with spans ranging from 20 ft to 65 ft. The motivation for the adoption of such a system is related to reflective cracking problems associated with traditional systems used for short-to-medium-span bridges. These traditional systems typically feature composite bridges constructed with adjacent precast voided slabs and adjacent box beams (Figure 2).



Figure 1. Poutre-Dalle System. Reprinted with permission from Matiere. From their website at <https://www.matiere-tp.com/beam-slab>.

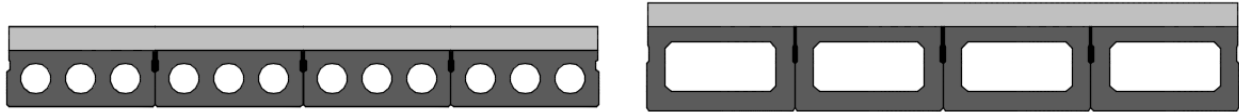


Figure 2. Voided Slab and Adjacent Box Beam Systems

One of the causes that can lead to reflective cracking is the transverse bending of the bridge when subject to concentrated loads such as vehicular loads (Figure 3). The only resisting mechanism against interface bond failure if transverse post-tensioning is not applied in the adjacent box or voided slab system is the tensile bond strength between the precast beams and the grout in the shear keys. The Poutre-Dalle system offers two improvements with respect to resistance against reflective cracking caused by transverse bending. First, it provides a thicker cast-in-place concrete topping over the longitudinal joints, and second, it offers a horizontal interface in addition to the vertical interface between the precast and cast-in-place components. The combination of these two interfaces emulates monolithic construction while preserving the benefits of prefabricated elements. In addition, the transverse hooked bars help arrest any potential cracks over the longitudinal joint or at the interface between the precast web and the cast-in-place topping.

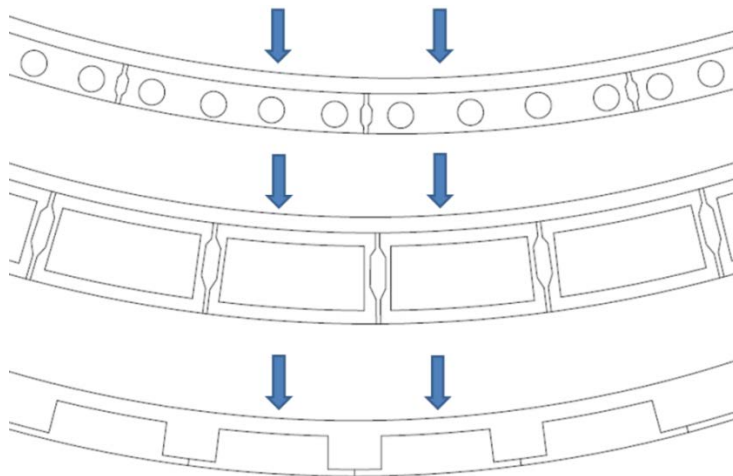


Figure 3. Deformed Shapes in Transverse Direction

Inspired by the Poutre-Dalle systems observed in France, engineers in Minnesota developed a similar system, which featured the same precast inverted T-beam shape and the extended transverse bars. The 180° hook at the ends of the transverse bars was changed to a 90° hook as shown in Figure 4(a). This was done to allow the placement of a “drop-in” reinforcing cage over the trough area to serve as additional reinforcement in the region above the longitudinal joint (Figure 4(b)). This system was targeted for implementation in the state of Minnesota for bridges with spans ranging from 20 ft to 65 ft. The first two bridges built with this system are located in Center City, Minnesota and Waskish Township, Minnesota (Hagen et al., 2005).

Over the course of seven years (2005 to 2012), researchers at the University of Minnesota investigated a variety of issues related to the design and construction of this new system. These

issues included studies on reflective cracking, crack control reinforcement, composite action, transverse live load distribution, restraint moments, skew effects, and stresses at the end zones. This research was presented in a series of technical reports. Most of these reports were prepared for the Minnesota Department of Transportation (MnDOT) (Hagen et al., 2005, Bell et al., 2006, Smith et al., 2007, Smith et al., 2008, Dimaculangan and Lesch, 2010), and one of them was prepared for the National Cooperative Highway Research Program (NCHRP) (French et al., 2011).



(a)



(b)

Figure 4. (a) Photograph of the Bars in the Precast Inverted T-beam, (b) Photograph of the Reinforcement Cage Installed Above the Precast Longitudinal Joint (Hagen et al., 2005). Reprinted with permission.

The inverted T-beam system developed in Minnesota was implemented on twelve bridges between 2005 and 2011 (Dimaculangan and Lesch, 2010). During this time the original concept underwent a number of modifications to improve performance in different design generations. To determine the effect of these design modifications on performance, a series of field inspections was done for five existing inverted T-beam bridges (Dimaculangan and Lesch, 2010). Field inspections were conducted using two separate, but related, procedures: crack mapping and core examinations. Figure 5 shows a crack map and the locations where the cores were extracted for Bridge No. 33008 near Mora, Minnesota. Cores 1 and 2 revealed a full-depth reflective crack and a shrinkage crack that extended $\frac{1}{2}$ in from the surface, respectively. Cores 3

and 4 revealed a 5¼-in deep reflective crack from the joint and a 3½-in deep shrinkage crack from the surface. Figure 5 suggests that the longitudinal and transverse surface cracking is extensive. Although the inverted T-beam system showed promise with respect to addressing reflective cracking concerns compared to the traditional voided slab system, the fabrication challenges presented by the extended transverse bars and the surface cracking observed in Minnesota’s bridges prompted the need for additional research.

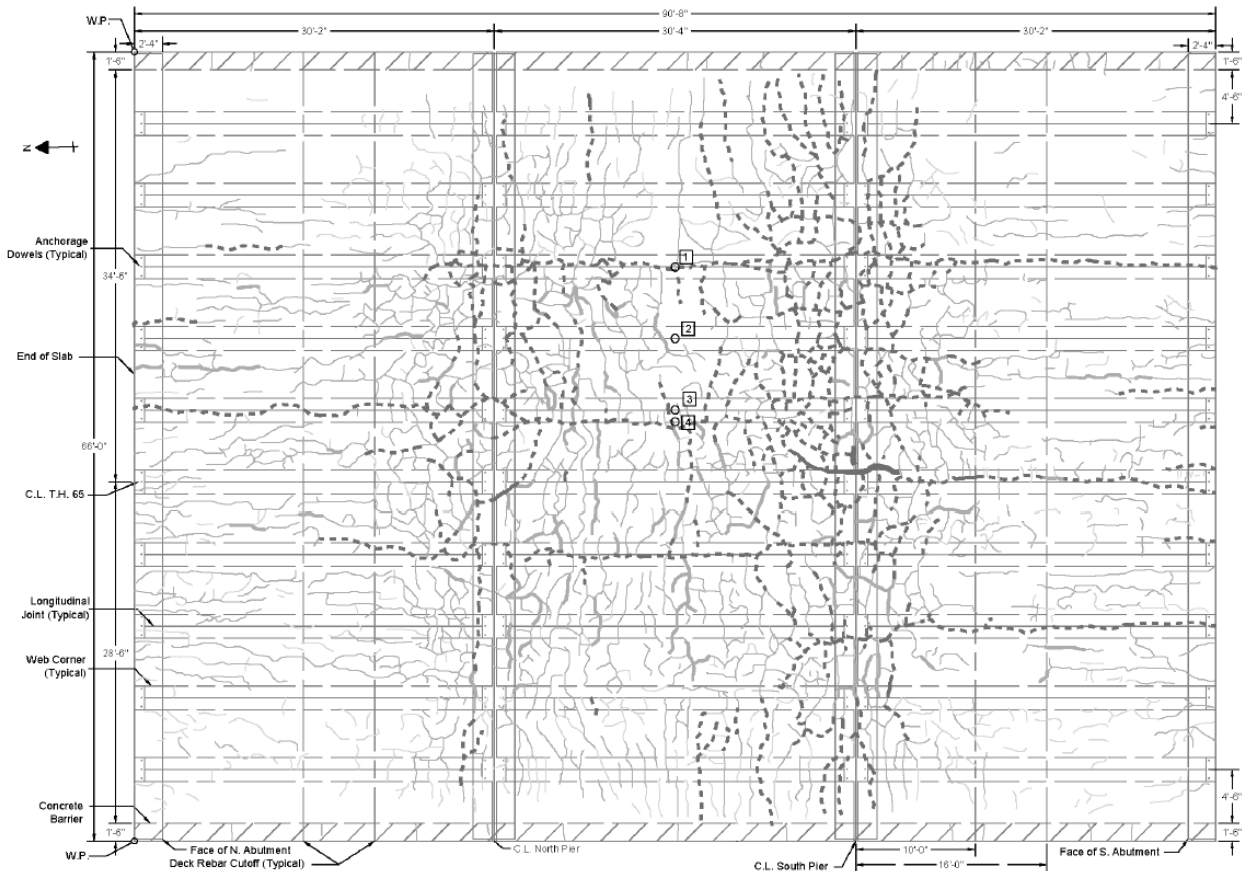


Figure 5. Crack Map for Bridge No. 33008, Inspection No. 3, June 16 and August 10, 2011, with Core Specimen Locations Indicated (Halverson et al., 2012). Reprinted with permission.

PURPOSE AND SCOPE

Being aware of reflective cracking problems present in short-to-medium-span bridges built with adjacent voided slabs and adjacent box beam systems, the Virginia Department of Transportation (VDOT) expressed interest in implementing the precast inverted T-beam system for the first time in Virginia. The application was a bridge replacement project near Richmond, Virginia, on US 360 and featured four bridges (Figure 6). Three of these bridges were targeted to be replaced with the traditional adjacent voided slab system and one of them with the new inverted T-beam system. In addition, the bridge that was targeted for replacement using the inverted T-beam system (B607) was identical in terms of number of spans, span lengths, bridge width, traffic volume and environmental conditions to one of the neighboring bridges, which was scheduled to be replaced using the traditional adjacent voided slab system (B608). Both were

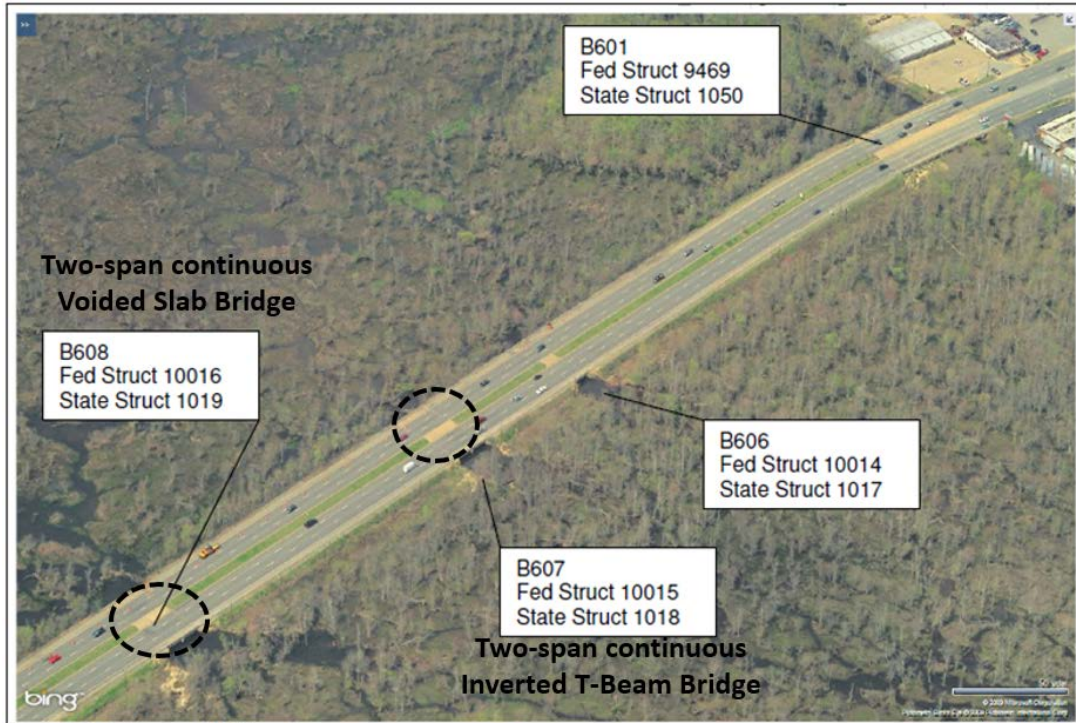


Figure 6. Aerial View of the Site Featuring Four Bridge Replacements (Hill and Lowe, 2010)

two-span continuous bridges with span lengths of approximately 43 ft (Figure 7). This provided an opportunity to observe the relative performances of these two bridges over time. There are multiple objectives of this project, and they are presented in the following sections. Other aspects of the investigation will be presented in Part II of this report.

Investigation of Cross-Sectional Shape and Transverse Connection

The most pressing issue of interest to VDOT was that related to reflective cracking. The objective was to build on Minnesota’s experience and investigate modifications to the inverted T-beam system that would lead to more durable, crack resistant and economical bridges. The scope of work to achieve this objective included performing a 3-D finite element analysis of the US 360 Bridge to quantify transverse bending demands and testing various cross-sectional shapes and transverse connections to investigate their performance with respect to transverse bending and reflective cracking. The alternative cross-sectional shapes and transverse connections were developed with the purpose of emulating monolithic construction, but without the need to extend transverse bars through the formwork, which provided a challenge for the precast fabricator during form installation and removal.

Optimization of Topping Concrete Mixture Design

Differential shrinkage is believed to be one of the causes of deck cracking in composite bridges. A study of shrinkage and creep properties of seven different deck mixtures was carried out with the goal of identifying a mixture whose long terms properties would reduce the

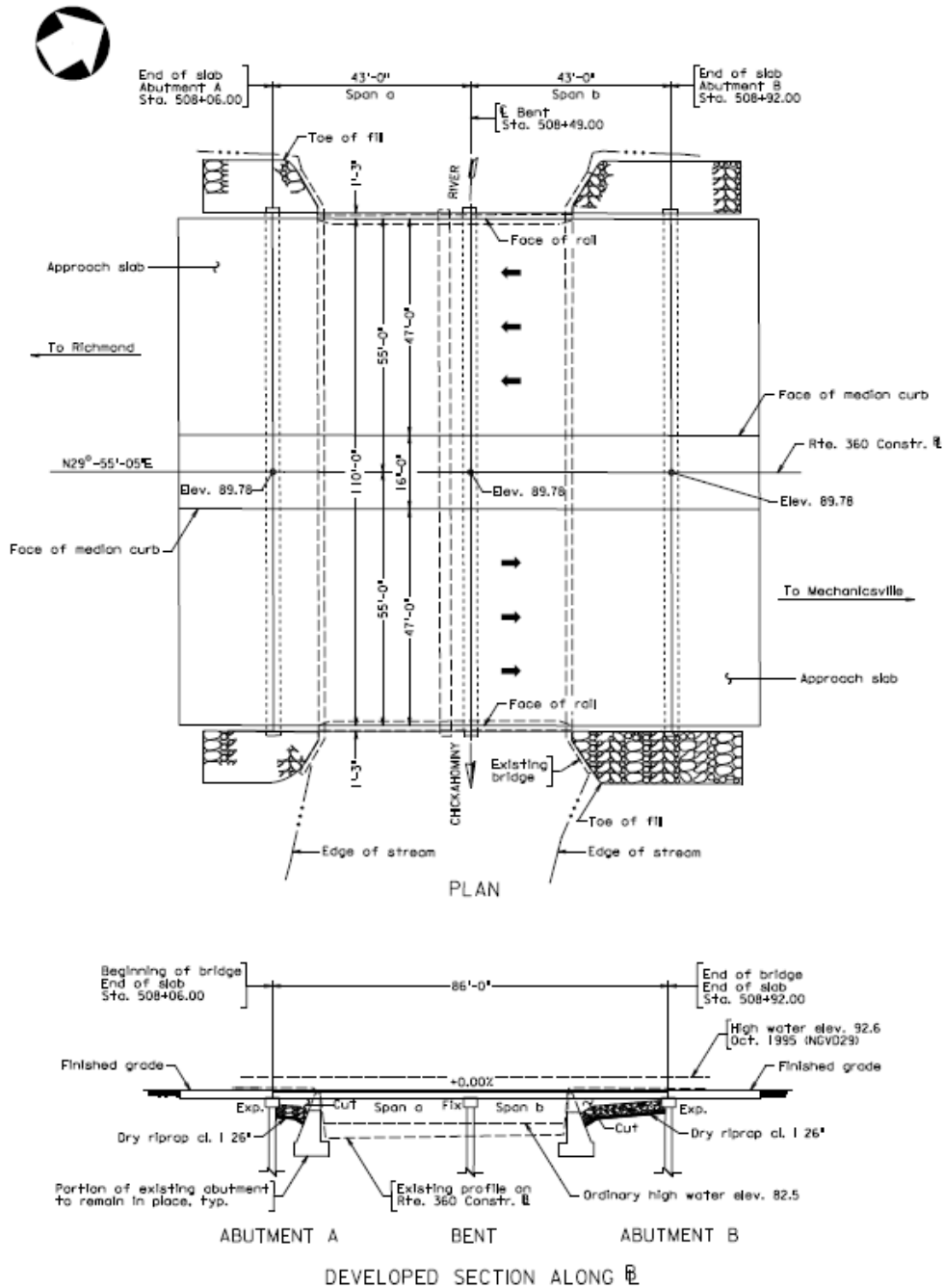


Figure 7. Preliminary Plan and Elevation of the US 360 Bridge Over the Chickahominy River (Hill and Lowe, 2010)

likelihood of deck cracking. A mixture with low shrinkage and high creep was expected to be most resilient to restrained shrinkage cracking. Short-term properties of compressive strength, tensile strength, and modulus of elasticity were also studied. Saturated lightweight coarse aggregates and fine aggregates were considered to have potential to reduce shrinkage, and were included in the study.

Composite Action

The unique interface between the precast inverted T-beams and the cast-in-place topping prompted the need to investigate the capability of the composite bridge to develop full composite action by relying solely on the cohesion between the two interfaces. The purpose of this study was to explore the need for extended stirrups for horizontal shear transfer by performing a full-scale test and subjecting a typical composite bridge cross-section to service and strength level design forces. The goal was to determine if the proposed composite bridge system can develop its nominal flexural strength without incurring any slip at the interface.

METHODS

This part of the final report deals with the three areas of study with laboratory testing components: the transverse connection study, the cast-in-place deck mixture optimization study, and the composite action study. The methods used in each are presented in the following sections.

Investigation of Cross-Sectional Shape and Transverse Connection

Analytical Study

Two finite element models of the US 360 Bridge were created in Abaqus (2012) to determine the worst-case transverse bending moment. One model featured precast inverted T-beams with straight webs and the other included precast inverted T-beams with tapered webs. To obtain the maximum transverse bending moment in the bridge, a linear-elastic analysis, which is appropriate up to the initiation of cracking, was performed using 3-D solid elements and uncracked concrete properties for both the precast and cast-in-place components. The quantification of the worst-case transverse bending moment was done by systematically placing the live load (combination of truck and lane load or tandem and lane load) on the bridge and by monitoring the magnitude of the transverse moments. The stresses created in the cast-in-place topping due to design live loads were smaller than the modulus of rupture regardless of the mesh size. The bond between the precast inverted T-beams and cast-in-place topping was assumed to be a perfect bond. The worst-case transverse bending moment, including the dynamic load allowance, was determined to be 14.5 ft-kips/ft.

Figure 8 illustrates the two-way plate bending behavior of the US 360 Bridge superstructure when subject to concentrated loads such as truck wheel loads. The transverse section demonstrates the effect of transverse bending. Figure 9 shows a close-up view of the longitudinal joint area, which is the most vulnerable to cracking as a result of transverse bending, because the presence of a joint between the precast beams creates a weakened plane.

Figure 10 shows how the effects of transverse bending on the bridge can be investigated by using a simply supported beam setup in the laboratory. Figure 11 illustrates the orientation of principal stress vectors in the full bridge model and in the sub-assembly model for the case when the precast inverted T-beam has tapered webs. As can be seen from the similarity of the

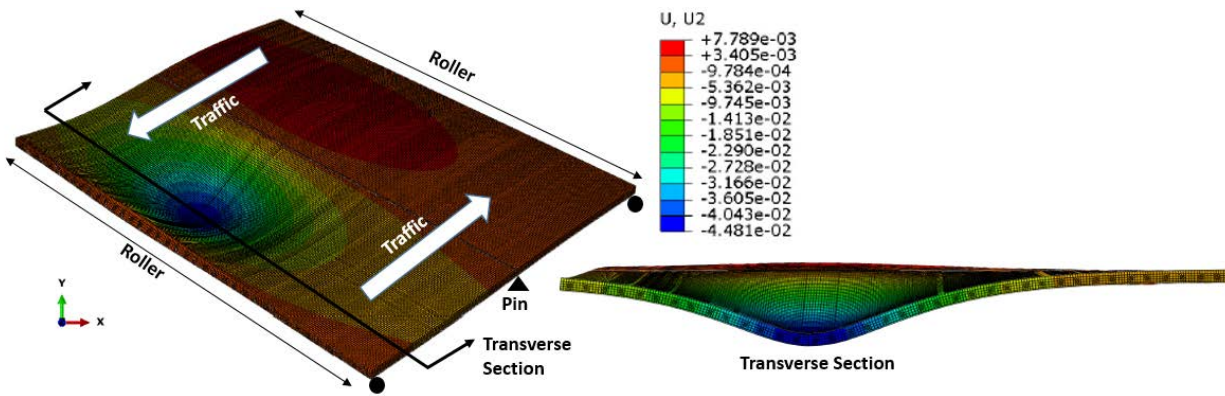


Figure 8. Isometric View of Plate Bending in Bridge Deck and a Transverse Section (Deformed Shape units - in)

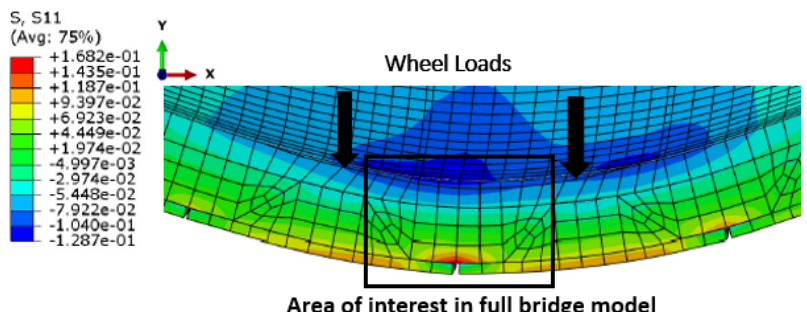


Figure 9. Transverse Normal Stress Contours (S11) Around the Longitudinal Joint in the Full Bridge Model (units – ksi)

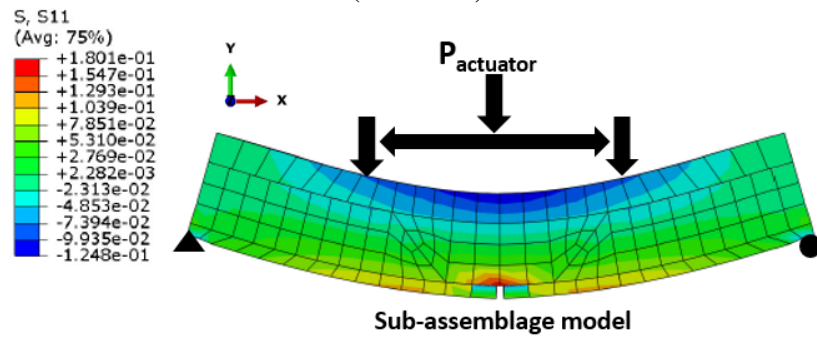


Figure 10. Transverse Normal Stress Contours (S11) Around the Joint in the Sub-Assemblage Specimen Model (units – ksi)

orientation of principal stress vectors in both models, the simply supported sub-assembly specimen can represent the stress condition around the longitudinal joint in the full bridge fairly well. In both models, the orientation of the principal tensile stress vectors below the neutral axis is horizontal, which indicates that normal stresses dominate over shear stresses.

Figure 12 illustrates the similarity in the orientation of principal stress vectors in the full bridge model and the sub-assembly model when the precast webs are straight rather than tapered. Because the orientation of principal tensile stress vectors below the neutral axis is horizontal, the resistance against cracking at the vertical interface between the precast beam and the cast-in-place concrete topping in the case when the precast beam has tapered webs is

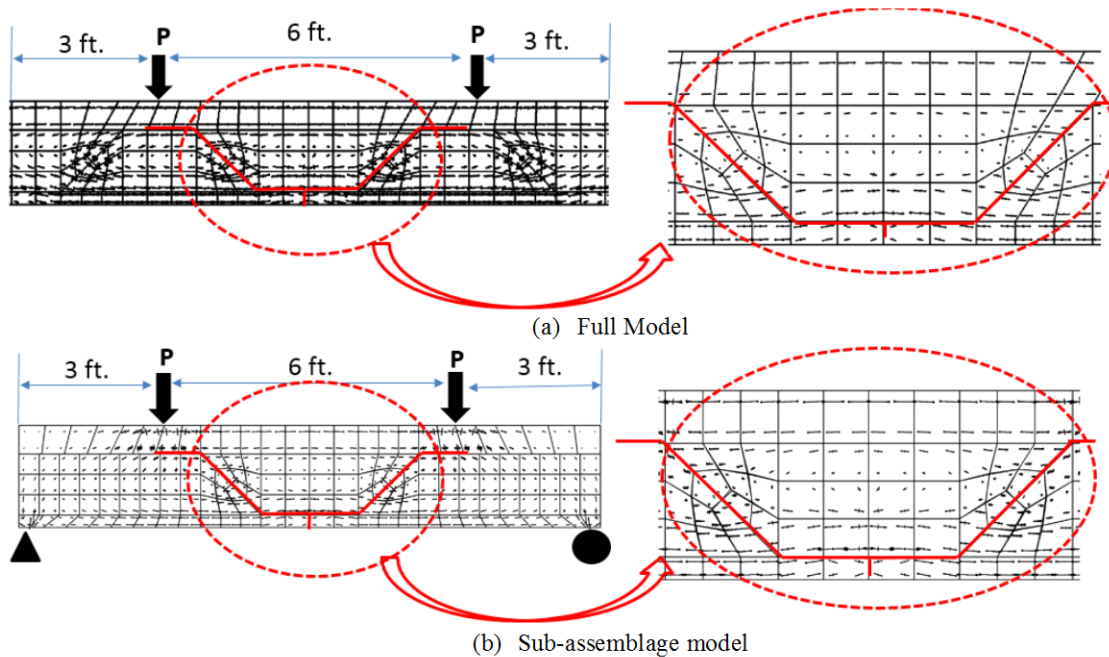


Figure 11. Principal Stress Vectors, (a) Full Model, (b) Sub-Assembly Model for an Inverted T-Beam With Tapered Webs; Solid Red Line Denotes Precast to Cast-in-Place Interface

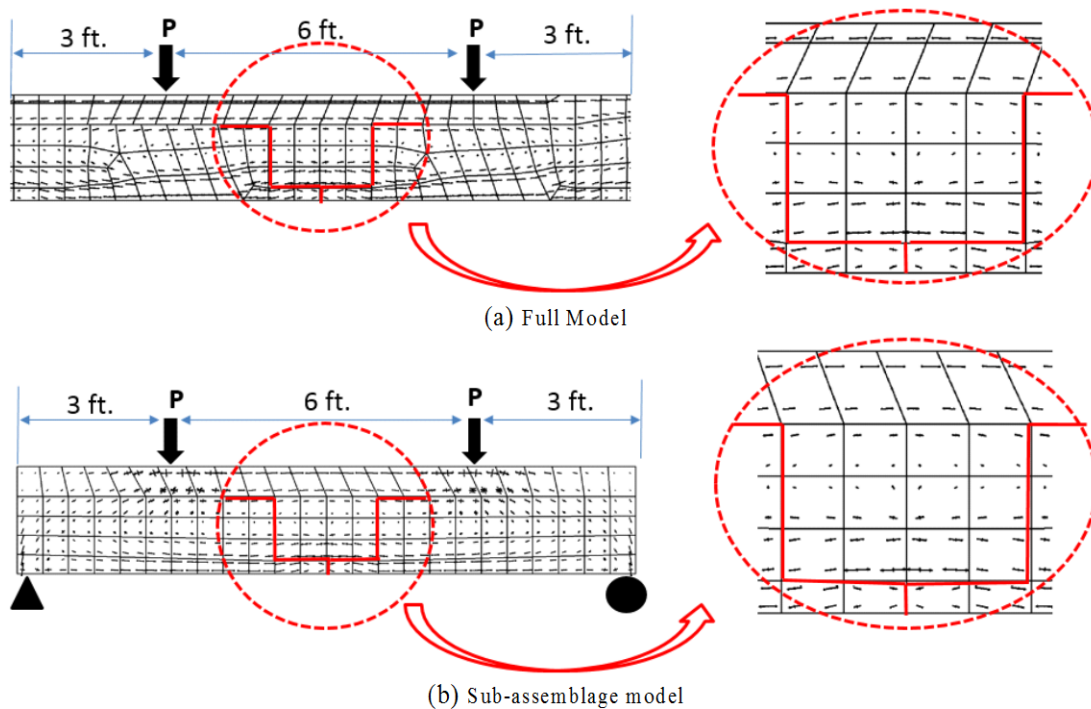


Figure 12. Principal Stress Vectors, (a) Full Model, (b) Sub-Assembly Model for an Inverted T-Beam With Vertical Webs; Solid Red Line Denotes Precast to Cast-in-Place Interface

provided by the combination of the shear and tensile strength of the bond. Conversely, in the case when the precast beam has straight webs, the resistance against cracking at the vertical

interface is provided predominantly by the tensile strength of the bond. Because the shear strength of an interface between two concretes cast at different times is higher than its tensile strength, the precast inverted T-beam with tapered webs promises to provide an enhanced resistance against cracking caused by transverse bending.

Because the simply supported sub-assembly specimen could replicate fairly well the stress state around the longitudinal joint observed in the full bridge model, several sub-assembly specimens were tested to compare their capacities in transverse bending with that demanded during service.

Experimental Investigation: Phase I

Figure 13 illustrates the concept behind the selection of the simply supported beam setup, which features two adjacent precast inverted T-beams and the associated concrete topping. The precast web was extended to replace the precast flanges at the supports to create a better bearing condition. The two point loads represent either tandem loading or HL-93 truck loading. Figure 14 shows a photograph of the test setup featuring a loading frame, actuator, spreader beam and two steel beams to provide supports for the test specimens. The two-point loading was applied by distributing the actuator load via the spreader beam to two tire prints. This loading arrangement created a region of constant moment and zero shear due to actuator loads in the region around the longitudinal joint, which is consistent with the fact that the orientation of

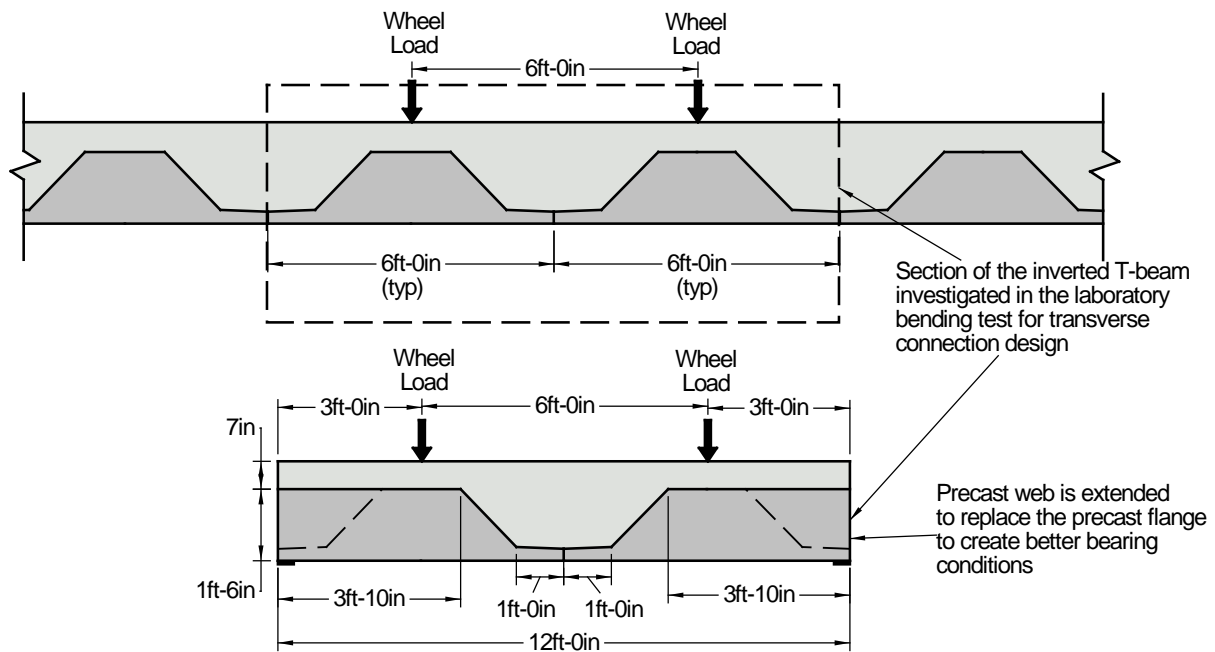


Figure 13. Sub-Assembly Test Specimen Concept



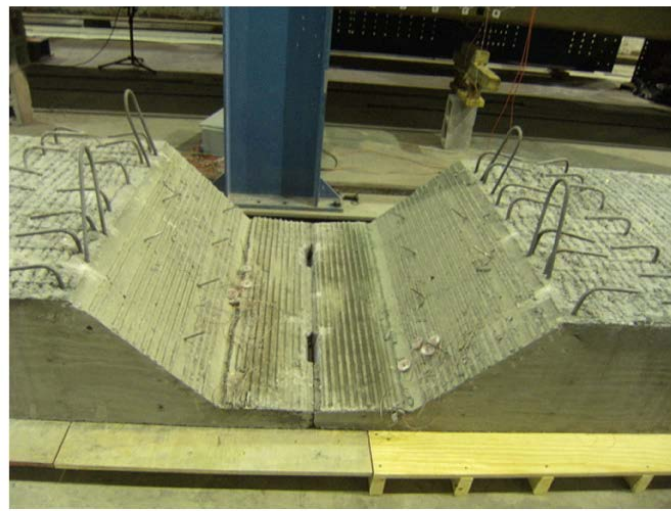
Figure 14. Photograph of Test Setup

principle tensile stress vectors in the full bridge model was mainly horizontal. The specimens were supported on 6-in wide by 0.75-in thick neoprene bearing pads. The superstructure for the two-span continuous US 360 Bridge was designed per AASHTO LRFD Bridge Design Specifications (2013) and the reinforcement for the sub-assembly specimens was selected accordingly. A finite element model of the sub-assembly test specimen was used to determine the actuator force (“wheel load” in Figure 13) that would create the worst-case transverse bending moment during service computed from the finite element model of the full bridge. This load was found to be 27 kips and is in addition to the self-weight of the test specimen.

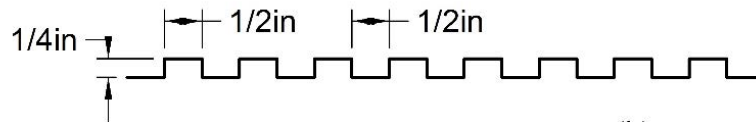
The design compressive strength at 28 days for the cast-in-place concrete topping and precast beams were $f'_c = 4,000$ psi and $f'_c = 8,000$ psi, respectively. All mild reinforcing steel was ASTM A615, Grade 60, deformed bare steel. Prestressing strands were ASTM A416, Grade 270, uncoated, low-relaxation strands. The prestressing strands in the test specimens were not prestressed because they do not have a significant influence on the behavior of the specimens in the transverse direction.

All surfaces of the precast inverted T-beams in contact with the cast-in-place topping were roughened in the longitudinal direction of the bridge to a 1/4-in amplitude to improve bond with the goal to emulate monolithic action in the transverse direction. The roughened surface in the side of the webs and the top of the precast flange was created by introducing grooves in the wooden formwork. The roughened surface at the top of the web was created by raking the fresh concrete immediately after placement to a 1/4-in amplitude. Figure 15(a) shows a photograph of the roughened surface in the precast members. Figure 15(b) shows the profile of the corrugated wood forms used to create the roughened surface on the side of the webs and top of the precast flange. An alternative profile is shown in Figure 15(c) and features corrugations with tapered sides, which are intended to facilitate the removal of forms. Set-retarding chemicals used on the

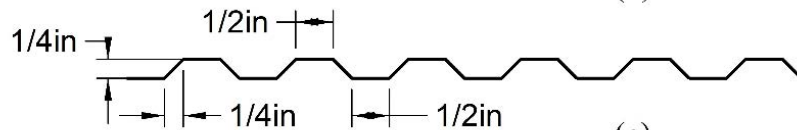
surface to create an exposed aggregate finish may be another way of creating an acceptably rough surface.



(a)



(b)



(c)

Figure 15. (a) Photograph of Roughened Surface, (b) Profile of Corrugated Wood Forms Used to Create the Roughened Surface, (c) Alternative Profile

During a trial concrete placement, it was observed that concrete did not flow all the way to the edge of the precast flanges. This was attributed to the fact that the flanges were formed on all sides without providing any air pressure relief during concrete placement. To correct this, an air relief strip was provided in the subsequent pours. In addition, coarse aggregates were changed from No. 57 stone to No. 78 stone to facilitate the flow of fresh concrete through the 3-in precast flange. Figure 16 shows the two precast pieces that were used in constructing the trial specimen. As can be seen, the shape of the flange could not be formed as intended. However, this specimen was tested to see how such a specimen with incomplete or damaged flanges would perform, in case situations like this were to occur during the fabrication of precast inverted T-beams.

Investigation of Two Precast Beam Cross-sectional Shapes

In this experimental study, two cross-sectional shapes were investigated. These are shown in Figure 17. The first cross-sectional shape is similar to the original French detail and also to the one used by MnDOT. It features a precast inverted T-beam with straight vertical



Figure 16. Trial Specimen With Straight Web, Extended Bars, and Incomplete Flanges

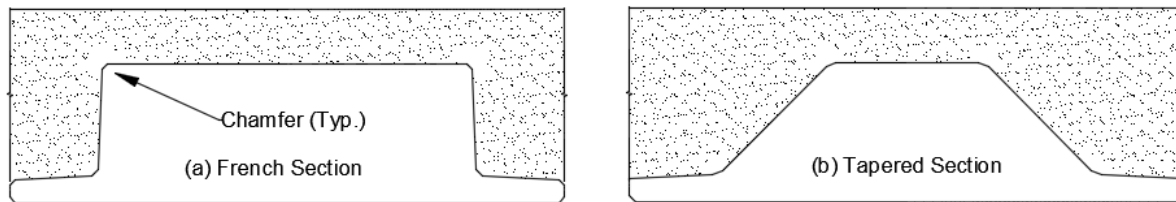


Figure 17. Two Cross-Sectional Shapes

webs. In the second cross-sectional shape, the webs of the precast inverted T-beam were tapered with the purpose of providing a higher bond strength against normal transverse tensile stresses at the interface of cast-in-place topping to the precast web. As can be seen from Figures 11 and 12, when transverse bending takes place in the bridge, normal tensile stresses are created in the transverse direction below the neutral axis in the precast web region. In the cross-sectional shape with the straight webs, the resistance against interface bond failure at the precast web is mainly limited to the bond strength in tension between the precast web and cast-in-place concrete topping. This phenomenon is described in Figure 18(a)-(d). Figure 18(a) and (b) illustrate the application of the transverse tensile stresses at the interface between precast web and cast-in-place topping in the systems with a straight precast web and tapered precast web, respectively. In both systems, the interface was intentionally roughened as described earlier. Figure 18(c) and (d) zoom in on a typical roughened surface pattern and illustrate the mechanisms that resist interface bond failure.

In the precast beam with straight webs, such a resisting mechanism consists primarily of the tensile bond strength between the precast and cast-in-place components and slightly on the shear bond strength at the horizontal surfaces of the corrugated pattern (Figure 18(c)). In the precast beam with tapered webs, the resisting mechanism relies on the combination of the shear and tensile bond strengths between the two components as well as on the mechanical interlock offered by the roughened surface in the tapered webs. Figure 18(e) illustrates the resistance

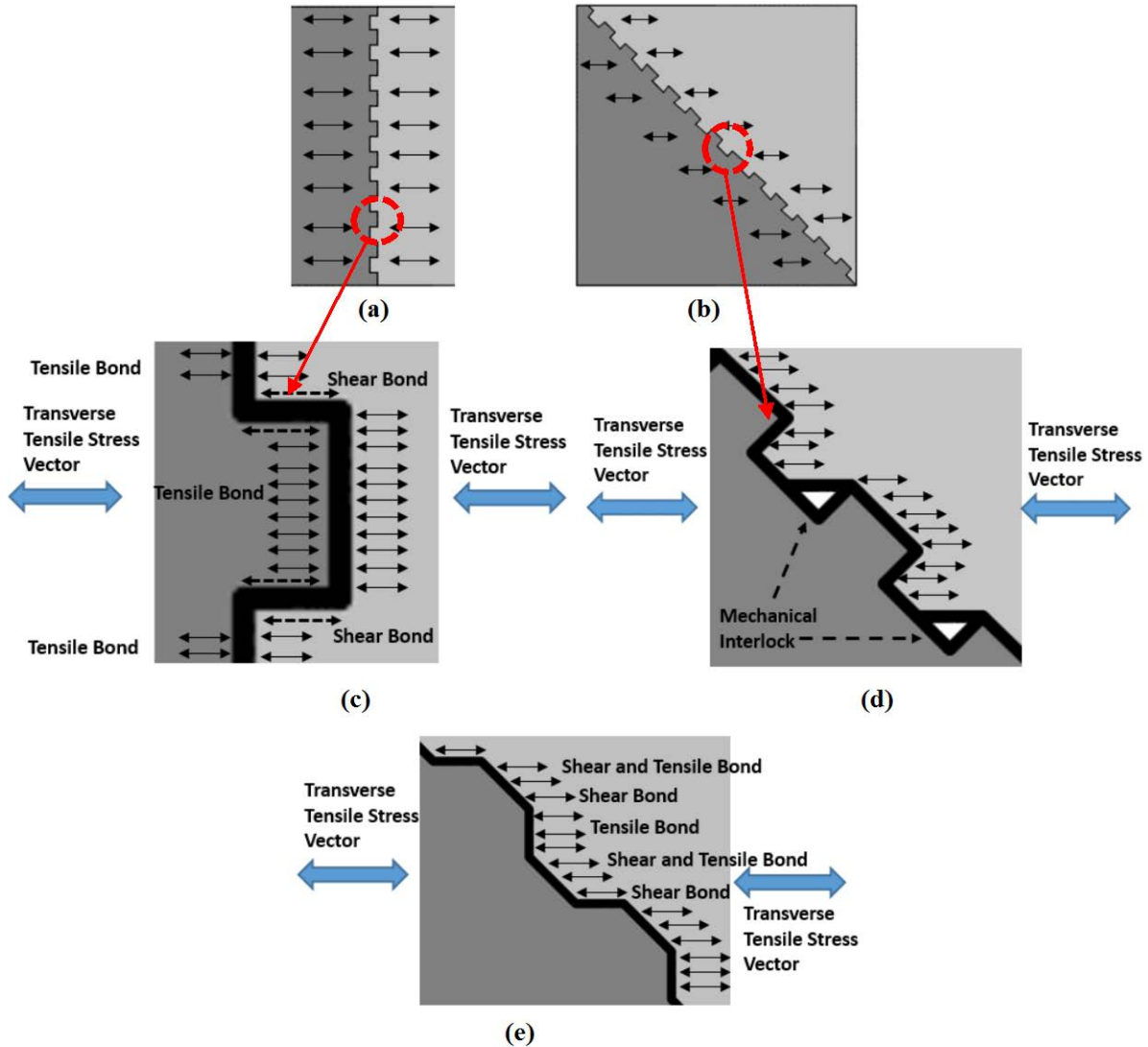


Figure 18. Transverse Tensile Stress Vectors, (a) Straight Web, (b) Tapered Web, Resistance Against Transverse Tensile Stress Vectors, (c) Straight Web, (d) Tapered Web With Roughened Surface, (e) Tapered Web With Alternative Roughened Surface

against interface bond failure in a precast beam with tapered webs, but with the alternative roughened surface profile illustrated earlier. In this case, the mechanical interlock between the precast web and cast-in-place topping is lost; however, the interface bond strength against transverse bending is still likely to be higher than the system with straight precast webs, because the resisting mechanism consists predominately of the combined shear and tensile strength of the bond.

Investigation of Three Transverse Connections

Another key aspect of the inverted T-beam system is the connection between the precast components and cast-in-place topping in the transverse direction. Therefore, three different connection details were investigated as shown in Figure 19. The first connection detail is similar

to the one used by MnDOT, which features bars extended from the sides of the precast webs (Figure 19(a)).

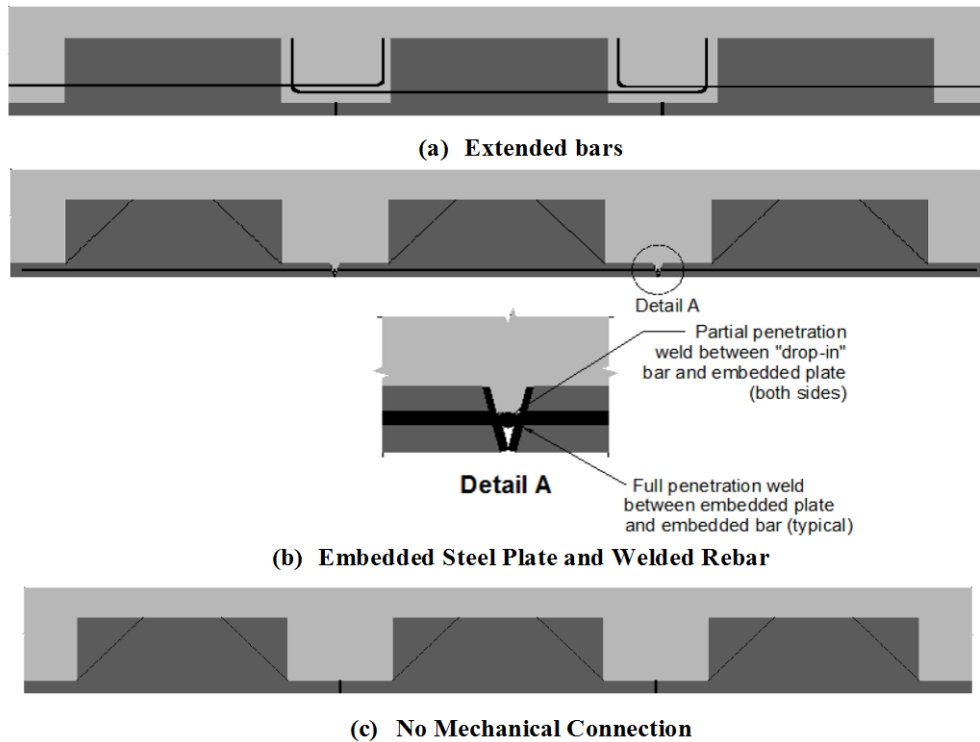


Figure 19. The Three Connections Investigated

The advantage of this detail is that the extended bars provide a mechanical connection between the precast component and cast-in-place topping. They also serve as a continuous tension tie in the transverse direction of the bridge. This detail minimizes the amount of work done at the construction site because the placement of concrete topping and reinforcing steel are the only activities required to deliver a bridge superstructure that will mimic monolithic construction in both directions. The disadvantage of this detail is that it creates challenges for the precast fabricator because the formwork for the webs of the precast inverted T-beams needs to accommodate the reinforcing steel protruding from the webs.

The second connection detail features discrete embedded steel plates in the precast flanges at 2 ft-0 in on center and welded reinforcing bars (Figure 19(b)). This detail does not have any reinforcing steel protruding from the precast webs. Instead, the precast flanges are connected by field welding a drop-in piece of reinforcing steel to each embedded steel plate. The embedded steel plate is inclined so that it can receive the drop-in bar as well as accommodate any differences in elevation due to camber variations between the precast inverted T-beams. Each embedded steel plate is welded to two reinforcing steel bars, which run for the entire width of the precast beam and are welded to the back of the embedded steel plate at each flange. Alternatively, each embedded steel plate can have its own set of transverse reinforcing steel bars welded to the back of it to provide some tolerance during fabrication. These transverse bars can then be tension-spliced with those coming from the embedded steel plate on the opposite flange. One advantage of this detail is the shift in location of the tension tie toward the

bottom of the precast element, where the maximum tensile stresses from transverse bending occur. This detail avoids having a complete separation between the precast flanges. Another advantage of this detail is the relative ease of forming the precast inverted T-beams when compared to the original French detail, in which the forms need to accommodate the protruding bars. One of the disadvantages is the field welding, which goes against the concept of accelerating bridge construction because it adds a relatively complex or time-consuming operation that needs to be done in the field.

The third connection detail relies solely on the bond between the cast-in-place topping and the precast inverted T-beam to emulate monolithic construction (Figure 19(c)). This detail is the simplest and most economical because it does not have any reinforcing steel protruding from the sides of the webs. It also does not have a mechanical connection between the precast members, which takes additional time in the field. Although all surfaces of the precast beam in contact with the cast-in-place topping should be intentionally roughened regardless of which detail is used, it is particularly important that this is done when the detail with no mechanical connection is selected. It is through the cohesion provided by the roughened surface that monolithic action is emulated.

Investigation of Five Sub-assembly Specimens

The two cross-sectional shapes and three connections were combined to produce a total of five specimens with different configurations and details. The depths of all specimens were selected such that they matched the overall depth of the bridge superstructure of the US 360 Bridge. The overall length of each specimen was 12 ft, which is equal to the width of two adjacent precast inverted T-beams. The width of the specimens was selected to be 4 ft - 0 in, which is a multiple of the spacing of the embedded plate connectors with the welded reinforcing bars (24 in) and the spacing of the extended bars from the precast webs (12 in). Table 1 shows the test specimen matrix for experimental Phase I.

Table 1. Test Specimen Matrix for Experimental Phase I

Specimen ID	Cross-sectional Shape	Connection	Transverse Bottom Reinforcement in CIP Trough	Transverse Bottom Reinforcement in Precast	Loading
Trial	Straight web	Extended bars	No. 6 at 12 in plus No. 4 stirrups at 12 in	No. 6 at 12 in hooked bars plus No. 3 stirrups at 18 in	¼ point
1	Straight web	Extended bars	No. 6 at 12 in plus No. 4 stirrups at 12 in	No. 6 at 12 in hooked bars plus No. 3 stirrups at 18 in	¼ point
2	Straight web	Embedded plate and welded rebar	None	4-No. 6 bars	¼ point
3	Tapered web	Embedded plate and welded rebar	No. 3 at 12 in	4-No. 6 bars	¼ point
4	Tapered web	No connection	No. 6 at 12 in	No. 3 at 18 in	¼ point

Trial Specimen and Specimen No. 1

The trial specimen and Specimen No. 1 were identical with the exception that the precast flanges in the trial specimen were incomplete due to the absence of an air relief strip in the forms for the precast flanges. Both of these specimens are similar in concept to the detail used by MnDOT. Figure 20 provides information on the reinforcement details. The transverse bars in the precast flange were sized to support the weight of the wet cast-in-place concrete topping. The size and spacing of the hooked bars and the pre-tied cage were based on the recommendations by French et al. (2011). The remaining reinforcing steel in the cast-in-place topping was based on minimum requirements for temperature and shrinkage.

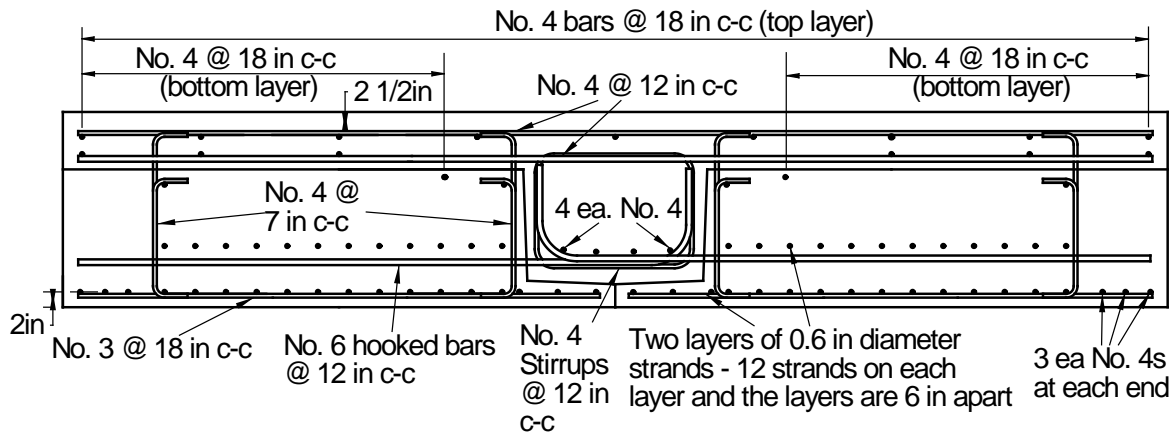


Figure 20. Reinforcement Details for Trial Specimen and Test Specimen No. 1

Specimen No. 2

This specimen had the same cross-sectional shape as Specimen No. 1. Reinforcement details are provided in Figure 21. There was no reinforcing steel protruding from the webs of the precast inverted T-beams. Instead, the flanges of the inverted T-beams were connected by welding a 6-in-long piece of reinforcing steel to an inclined steel plate and embedding the assembly in the precast flange. The size of the transverse bars in the precast flange was based on the transverse moment at service load, created as a result of live loads using allowable stress design principles and ignoring the contribution of concrete in tension. The allowable stress for the reinforcing steel was taken equal to 30 ksi. Reinforcing steel in the cast-in-place topping was based on minimum requirements for temperature and shrinkage.

Specimen No. 3

In this specimen, the connection between the precast flanges was identical to the one used in Specimen No. 2. Unlike Specimen No. 2, this specimen had a tapered cross-sectional shape. Another difference was that the bottom layer of deck steel in this specimen was detailed such that it followed the shape of the cast-in-place topping as opposed to the specimen with the straight web where this layer was straight. Similar to Specimen No. 2, the amount of transverse steel in the precast flanges was based on the transverse live load moment at service. The No. 3 bent bars at 12 in on center in the bottom of the cast-in-place topping were not relied upon when

calculating the transverse flexural strength of the specimen, but were provided as temperature and shrinkage reinforcement together with the top layer of straight No. 4 bars at 12 in on center. Reinforcement details are provided in Figure 22.

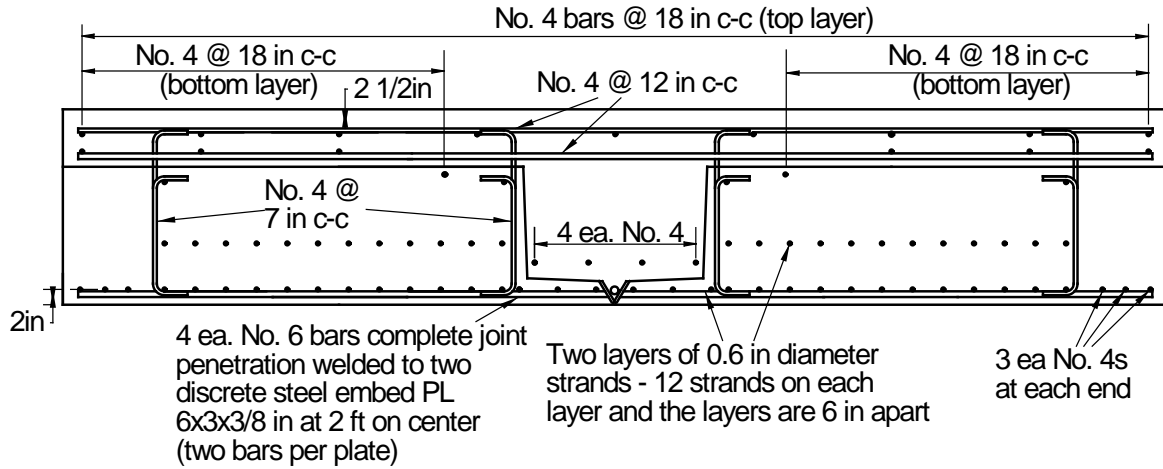


Figure 21. Reinforcement Details for Test Specimen No. 2

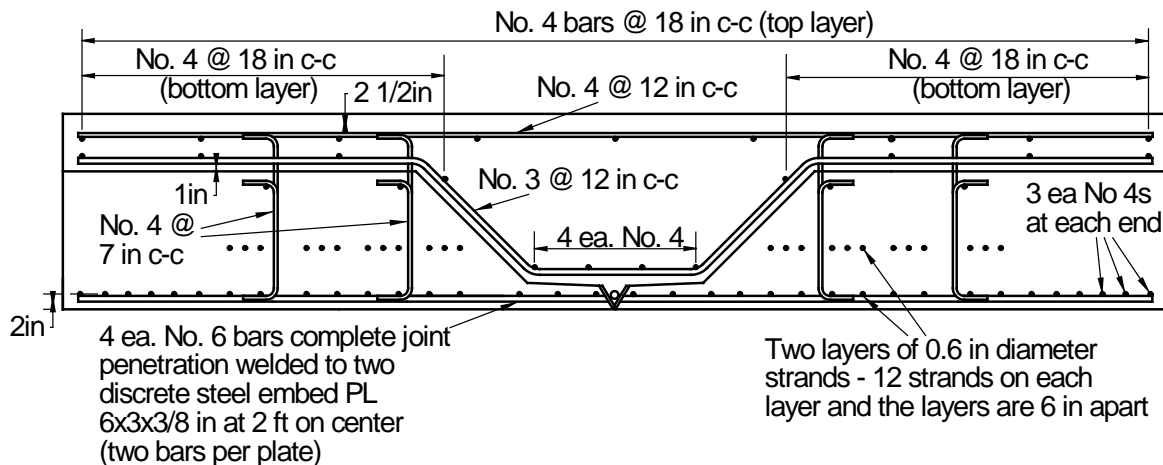


Figure 22. Reinforcement Details for Test Specimen No. 3

Specimen No. 4

Finally, the specimen shown in Figure 23 differs from the other specimens because it has no mechanical connection between the inverted T-beams and the cast-in-place topping. It is believed that composite action in the transverse direction will be achieved due to the bond between the roughened surface in the precast inverted T-beam and the cast-in-place concrete topping. Similar to Specimens No. 2 and No. 3, the transverse bottom steel in the cast-in-place topping was based on the transverse live load moment at service. However, the transverse reinforcement in the precast flanges was only designed to resist the weight of the wet cast-in-place concrete topping. In this specimen, a complete tension tie can be developed only if the tensile force resisted by the bottom layer of bars in the deepest portion of the cast-in-place topping (No. 6 at 12 in on center) can be transferred via a non-contact splice to the transverse

bars in the precast inverted T-beam (No. 3 at 18 in on center). Clearly, the weak link in this case is the flexural capacity of the composite section in the transverse direction provided by the No. 3 bars at 18 in on center.

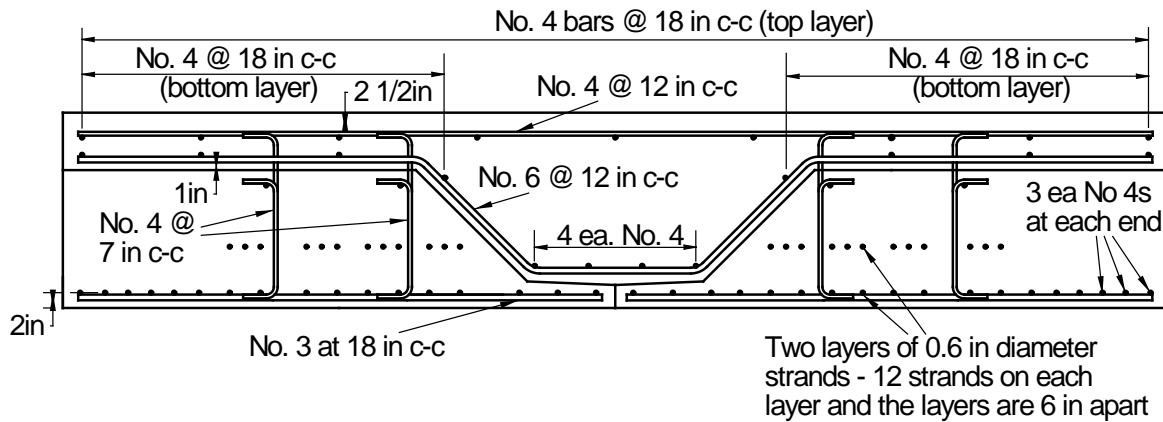


Figure 23. Reinforcement Details for Test Specimen No. 4

Test Protocol

Each specimen was loaded in increments of 5 kips up to 30 kips, which was slightly over the service level load (P_{service}) of 27 kips. Subsequently, the load was increased in 10-kip increments up to first cracking. First cracking load (P_{cr}) was taken equal to the actuator load that caused the first crack. The width of the first crack was recorded and the specimens were subjected to five cycles of loading, with the maximum load being the load that caused the first crack and the minimum load being equal to zero kips. At the end of five cycles, the crack width was re-measured to determine whether there was any increase in the crack width. The crack length was also monitored to determine whether the crack propagated as a result of the five load cycles. Then the specimen was subjected to three more load cycles and the crack measurement procedure was repeated. Monitoring of crack widths and propagation was done for the ninth and tenth load cycles, at the end of which repeated loading was terminated if it was determined that there was no increase in crack width or any crack propagation. If, at the end of the tenth cycle, the specimen showed signs of crack growth or propagation, then the specimen was subjected to additional load cycles until crack stability was achieved. After the repeated loading was terminated, the specimens were loaded monotonically to failure (P_u) or until the capacity of the loading frame was reached. The capacity of the loading frame was 300 kips. The load step after the repeated loading was 10 kips and at every load step the crack width was recorded and the crack pattern was marked on the specimens.

Experimental Investigation: Phase II

Because the specimen with the tapered web and no mechanical connection exhibited satisfactory performance under the service level load, a second phase of experimental testing was undertaken to improve upon this detail while maintaining its simplicity. The first goal was to increase the failure load by increasing the area of transverse steel in the precast flanges. The size and spacing of these bars was selected such that they matched the area of the bent bars in the

cast-in-place topping. In this manner a continuous tension tie with the same strength would be provided along the entire transverse cross-section of the bridge, assuming that the non-contact splices would perform satisfactorily. The second goal was to investigate the performance of the region around the joint when the specimens were subjected to a combination of flexure and shear. To accomplish these goals, three additional specimens were tested. Table 2 shows the test specimen matrix for Experimental Phase II.

Table 2. Test Specimen Matrix for Experimental Phase II

Specimen ID	Cross-sectional Shape	Connection	Transverse Bottom Reinforcement in CIP Trough	Transverse Bottom Reinforcement in Precast Flange	Loading
5	Tapered web	No connection	No. 6 at 12 in	No. 6 at 12 in	¼ point
6	Tapered web	No connection	No. 4 at 6 in	No. 4 at 6 in	¼ point
7	Tapered web	No connection	No. 4 at 6 in	No. 4 at 6 in	Offset to induce shear

Specimen No. 5

This specimen is identical to Specimen No. 4 with the exception that the bent bars in the cast-in-place concrete and the transverse bars in the precast flanges consisted of No. 6 bars at 12 in on center. Reinforcement details for this specimen are provided in Figure 24. This specimen was loaded at ¼ points. The increase in bar size and reduction in spacing in the precast flanges was intended to provide an increase in the flexural capacity of the precast section in the transverse direction by replacing the No. 3 bars at 18 in on center with No. 6 bars at 12 in on center.

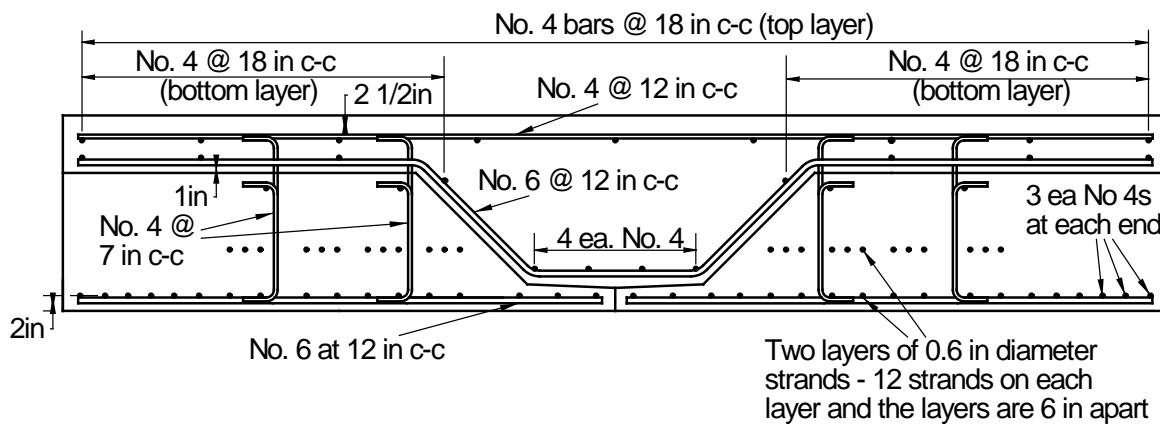


Figure 24. Reinforcement Details for Test Specimen No. 5

Specimen No. 6

This specimen is also identical to Specimen No. 4 with the exception that the bent bars in the cast-in-place concrete and the transverse bars in the precast flanges consisted of No. 4 bars at 6 in on center. Reinforcement details for this specimen are provided in Figure 25. This change was also intended to provide an increase in the flexural capacity of the precast section in the

transverse direction by replacing the No. 3 bars at 18 in on center with No. 4 bars at 6 in on center. The area of steel provided by No. 4 at 6 in on center is similar to the area provided by No. 6 at 12 in on center (0.40 in^2 per ft and 0.44 in^2 per ft, respectively). Both of these areas were large enough to resist the transverse bending moment due to live loads. This specimen was tested to determine the influence of smaller reinforcement spacing.

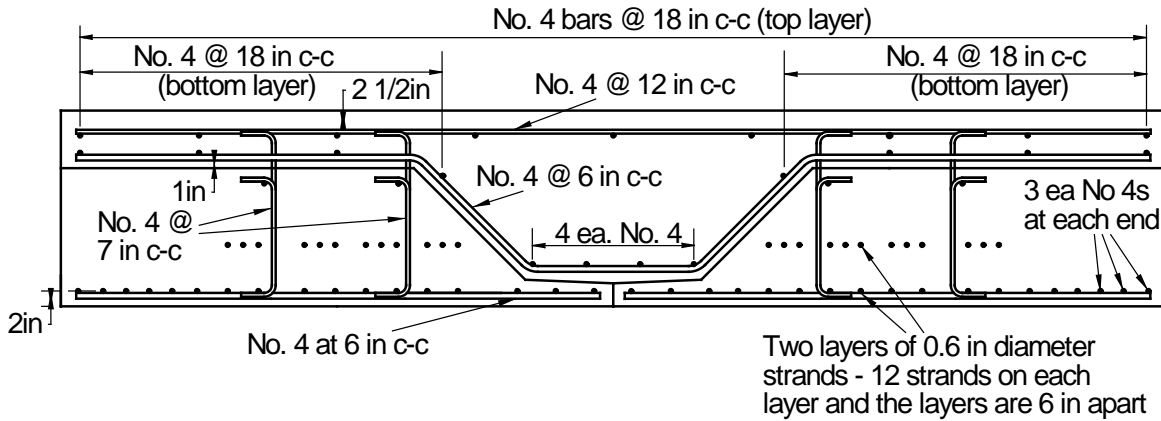


Figure 25. Reinforcement Details for Test Specimens No. 6 and No. 7

Specimen No. 7

This specimen was identical to Specimen No. 6 with the exception that the loading arrangement was as shown in Figure 26. This specimen was tested to observe the performance of the joint between the precast inverted T-beams when subject to a combination of shear and flexural stresses. As stated earlier, the predominant stresses in the transverse direction in the region around the joint for the US 360 Bridge near Richmond, VA, were flexural in nature. However, other situations may exist that create shear stresses around the joint that may not be negligible. Reinforcement details for this specimen are provided in Figure 25.

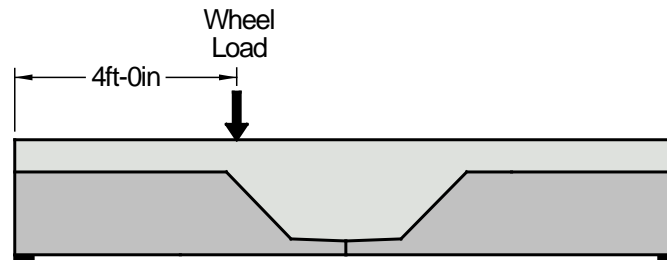


Figure 26. Loading Arrangement for Specimen No. 7

Optimization of Topping Concrete Mixture Design

Experimental Evaluation

The cracking that was seen in the Minnesota inverted T-beam bridges (see Figure 5) was, at least partially, attributed to restrained shrinkage of the topping concrete. Since the precast inverted T-beams are typically at least 28 days old at the time the topping is placed, a

considerable amount of their shrinkage has already occurred. The newly placed topping shrinks more than the precast beams, and the beams restrain the shrinkage. This results in tensile stresses in the topping, which can lead to cracking. To reduce this problem, a topping mixture with low shrinkage was sought. Since creep helps to relieve the tensile stresses, high creep was also a desirable property in the topping concrete.

Seven deck mixtures were put through a battery of tests to investigate their short-term and long-term properties. The deck mixtures contained normal-weight and lightweight coarse and fine aggregates. The mixture proportions for each mix design are provided in Table 3. The cementitious materials that were used were fly ash and blast furnace slag. To increase the workability of the mixtures without increasing the water content, superplasticizer was used as needed. In addition, because bridge decks are structural components that are exposed to weather, an air-entraining admixture is typically used to improve durability when the deck is subjected to freeze-thaw cycles and deicing salts. Target material properties were as follows:

- Minimum compressive strength at 28 days = 4,000 psi
- Maximum coarse aggregate size:
 - normal-weight mixtures = No. 57 stone (1 in)
 - lightweight mixtures = $\frac{3}{4}$ in
- Minimum cementitious materials content = 635 lb/yd³
- Maximum water–cementitious materials ratio (w/cm):
 - normal-weight mixtures = 0.45
 - lightweight mixtures = 0.43
- Slump = 4 in to 7 in
- Air content = 6½% ± 1½%.

When a high-range water reducer (superplasticizer) was used, the upper limit on air content was increased by 1%. One batch was prepared for each concrete mixture design.

Short-term properties determined for the deck mixtures include compressive strength, splitting tensile strength, and modulus of elasticity. These short-term properties are useful in assessing the quality of concrete and the response to short-term loads such as vehicle live loads (Barker and Puckett, 2007). Sometimes these short-term properties are modified to account for the long-term effects. For example, the Age Adjusted Effective Modulus (AAEM) method (Bazant, 1972) accounts for the increase in strain due to creep of concrete under sustained loads by employing a reduced long-term modulus of elasticity. The compressive strength, splitting tensile strength and modulus of elasticity were determined in accordance with ASTM C39 (2010a), ASTM C496 (2010d), ASTM C469 (2010c), respectively. Tests were performed to determine the compressive strength and modulus of elasticity at 7, 14, 28, 56 and 90 days of age. Tensile strength was determined at 7, 28 and 90 days of age.

Typically, compressive strength, tensile strength and modulus of elasticity of concrete increase with age; however, in this paper the phrase long-term properties is used to describe shrinkage and creep properties of concrete. Shrinkage is considered to be a change in volume during hardening and drying under constant temperature, whereas creep is defined as an increase in strain over time under a constant stress. Shrinkage and creep tests were performed in

Table 3. Design Mixture Proportions for Topping Concrete

Mixture Proportions				
Constituent	NWC-FA lb/yd ³	NWC-SL1 lb/yd ³	SLWC-FA lb/yd ³	SLWC-SL lb/yd ³
Portland Cement	476	413	476	413
Fly Ash	159	0	159	0
Slag Cement	0	222	0	222
Water	286	286	273	273
Coarse Aggregate	1780	1780	901	901
Fine Aggregate	1034	1082	1357	1403
Total	3735	3783	3166	3212
Unit Weight	138	140	117	119
w/cm	0.45	0.45	0.43	0.43
Mixture Proportions				
Constituent	NWC-SLWF-SL lb/yd ³	NWC-SL2 lb/yd ³	NWC-SLWF lb/yd ³	
Portland Cement	382	382	635	
Fly Ash	0	0	0	
Slag Cement	254	254	0	
Water	261	286	261	
Coarse Aggregate	1733	1733	1733	
NW Fine Aggregate	666	1285	666	
LW Fine Aggregate	403	0	403	
Total	3699	3940	3698	
Unit Weight	137	146	137	
w/cm	0.41	0.45	0.41	

NWC-SL = normal weight coarse aggregate slag mixture 1, NWC-FA = normal weight coarse aggregate fly ash mixture, SLWC-SL = saturated light-weight coarse aggregate slag mixture, SLWC-FA = saturated light-weight coarse aggregate slag mixture, NWC-SLWF-SL = normal weight coarse aggregate with saturated light weight fine aggregates and slag, NWC-SL2 = normal weight coarse aggregate slag mixture2, NWC-SLWF = normal weight coarse aggregate with saturated light weight fine aggregate.

accordance with ASTM C 157 (2010b) and ASTM C 512 (2010e), respectively. Creep specimens were placed in a frame and loaded 7 days after casting and the applied load was maintained at approximately $0.4 f'_{c7}$ where f'_{c7} is the average cylinder compressive strength at 7 days). The time-dependent properties of concrete are influenced by the environmental conditions at the time of placement and throughout its service life (ACI 209, 2008). These properties are used in determining the structural effects of differential shrinkage and creep. ACI 209.2 (ACI 209, 2008) provides four models for calculating shrinkage and creep properties as a function of time. AASHTO (2013) has its own models for creep and shrinkage. ACI 209.2 states:

The variability of shrinkage and creep test measurements prevents models from closely matching experimental data. The within-batch coefficient of variation for laboratory-measured shrinkage on a single mixture of concrete was approximately 8% (Bazant, 1987). Hence, it would be unrealistic to expect results from prediction models to be within plus or minus 20% of the test data for shrinkage. Even larger differences occur for creep predictions. For structures where shrinkage and creep are deemed critical, material testing should be undertaken and long-term behavior extrapolated from the resulting data.

It should be noted that the tests performed on the deck mixtures described in this investigation were performed only on one batch for each mixture. It was outside the scope of study to investigate the repeatability and consistency of the results obtained from each mixture.

Composite Action Study

A full-scale composite beam representing the US 360 Bridge was tested with the purpose of investigating its performance under design service level and strength level moments and shears. To investigate the necessity of extended stirrups, half of the composite beam span featured extended stirrups, whereas the other half did not. Initially, extended stirrups were provided along the entire span of the precast beam; however, prior to the placement of the cast-in-place topping, the stirrups on one half of the span were cut off.

Figure 27(a) shows the cross-sectional dimensions of the composite section. Figure 27(b) shows the reinforcement details for half of the span that featured extended stirrups, whereas Figure 27(c) features the reinforcement details for the other half. All precast surfaces in contact with the cast-in-place topping were roughened. The tapered precast webs and the tops of the precast flanges were roughened in the longitudinal direction to enhance composite action in the transverse direction of the bridge. Full composite action in the transverse direction is desired to avoid delamination at the interface of precast beam to cast-in-place topping because of transverse bending caused by wheel loads. Figure 28 shows the roughened precast surfaces. The roughened surface on the tapered webs was created by using steel forms, the inside of which featured the pattern shown in Figure 29. The tops of the precast bottom flanges were roughened in the longitudinal direction by using a traditional 1/4-in rake finish. The top of the precast web was roughened in the transverse direction with a 1/4-in rake finish to enhance composite action in the longitudinal direction.

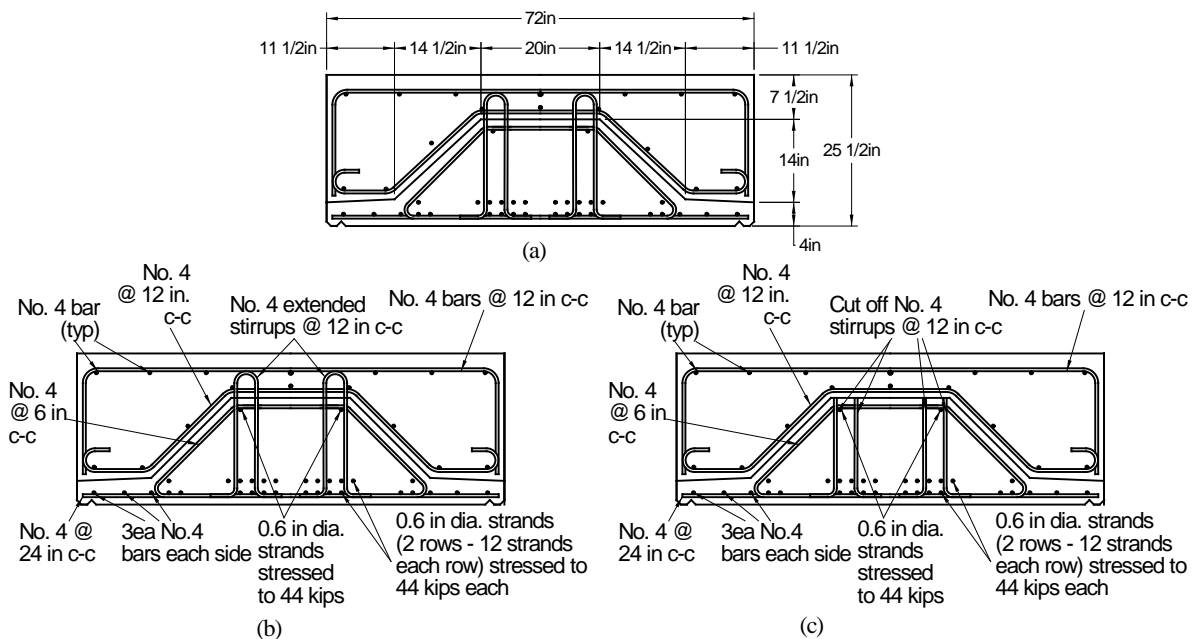


Figure 27. (a) Composite Beam Cross Section, (b) Half of the Span with Extended Stirrups, (c) the Other Half of the Span Without Extended Stirrups



Figure 28. Roughened Precast Surfaces

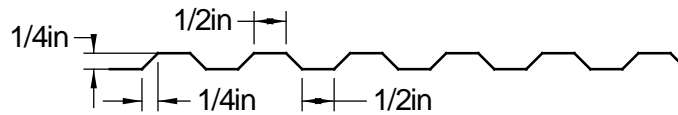


Figure 29. Roughened Surface Pattern in the Longitudinal Direction

Figure 30 shows the elevation of the composite beam and some of the instrumentation used to verify composite action. A displacement sensor (denoted WP-7) was used at mid-span with the purpose of comparing the load versus mid-span deflection curve obtained experimentally with that obtained analytically assuming full composite action. Displacement sensors were also used at quarter points (denoted WP-8 and WP-6) with the purpose of comparing the load versus quarter-span deflection curves of that half of the span that contained extended stirrups and that which had no extended stirrups. Identical load versus quarter-span deflection curves would serve as evidence that the presence of extended stirrups is not required to enhance composite action.

A photograph of the test setup is provided in Figure 31 that features the loading frame near mid-span. A 220-kip, closed-loop servo-controlled hydraulic actuator powered by a 30-gallons-per-minute hydraulic pump was used to load the composite system monotonically. A pin support was provided at one end of the beam and a roller support was provided at the other end to accommodate any potential longitudinal translation during testing. The pin support was provided by a solid, circular steel section that rested on an assembly of a semicircular steel pipe

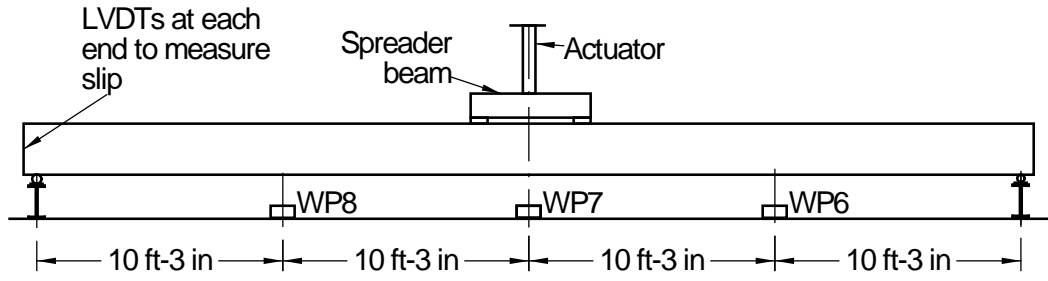


Figure 30. Drawing of Test Setup



Figure 31. Photograph of Test Setup

section and a channel welded together. A similar assembly was placed above the solid steel section and the beam was placed upon it. This created an assembly that allowed rotation but not longitudinal translation. At the other end of the beam, the roller support was provided by placing the pipe and channel assembly on top of the solid circular section, but not below. The circular section could roll on top of the support beam, which allowed rotation and longitudinal translation at the same time. The precast flanges at the ends of the precast beam were terminated 1 ft short of the end of the beam to prevent high flexural stresses in the precast flanges at the bearing points (such as abutments and intermediate supports). The cast-in-place topping for the tested full-scale beam followed the outline of the precast beam at the ends.

In addition to the displacement sensors, ten LVDTs were used to ensure that there was no slip during the various loading stages. Loss of composite action would be manifested as a relative slip between the precast and the cast-in-place components. Five LVDTs were used at each end (Figure 32) to capture any potential slip. The LVDTs at each end consisted of one installed at the interface between the top of the precast web and the cast-in-place topping, two installed at the interface between the precast flanges and the cast-in-place topping, and two others installed near the ends of the composite beam but on the sides at the interface between the precast flanges and the cast-in-place topping.



Figure 32. Location of LVDTs at the Ends of the Composite Beam to Measure Slip

Table 4 provides a summary of the moments and shears to which the individual precast inverted T-beams in the US 360 Bridge were expected to be subject. The moments and shears due to each load case are tabulated, and that information was used to calculate design moments and shears using Service I and Strength I load combinations (AASHTO, 2013). Three tests were performed with the purpose of simulating the maximum service level positive moment, the maximum strength level shear, the maximum strength level positive moment and the nominal moment capacity of the composite section. During the first test, the simply supported beam was subject to two point loads symmetrically located about mid-span (Figure 33(a)). The two-point loading was applied by attaching a spreader beam to the actuator and by supporting the spreader beam on two tire prints located 4 ft apart. The 4-ft spacing was intended to represent tandem axle spacing. The actuator load required to simulate the maximum service level positive moment was estimated to be 40 kips (20 kips on each tire print). During this test, the composite beam was expected to remain uncracked and behave elastically.

Table 4. Design Moments and Shear for Each Composite Beam at Service and at Ultimate

Load Case	Moment, ft-kip		Shear, kip	
Service (Service I)				
Self-weight of inverted Tee	$+M_{invT}$	173	V_{invT}	17
Self-weight of topping concrete	$+M_{deck}$	231	V_{deck}	22
Maximum positive live load moment	$+M_{live}$	297	V_{live}	45
Maximum negative live load moment	$-M_{live}$	219		
Positive superimposed dead load	$+M_{superD}$	60	V_{superD}	12
Negative superimposed dead load	$-M_{superD}$	107		
Total service load moment	$+M_{service} = 761$			
Ultimate (Strength I)				
Maximum positive factored moment	$+M_u$	1100	$V_{ucritical}$	138
Maximum negative factored moment	$-M_u$	516		

The purpose of the second test was to simulate the strength level design shear. The loading frame was moved from mid-span to the position shown in Figure 33(b). The actuator

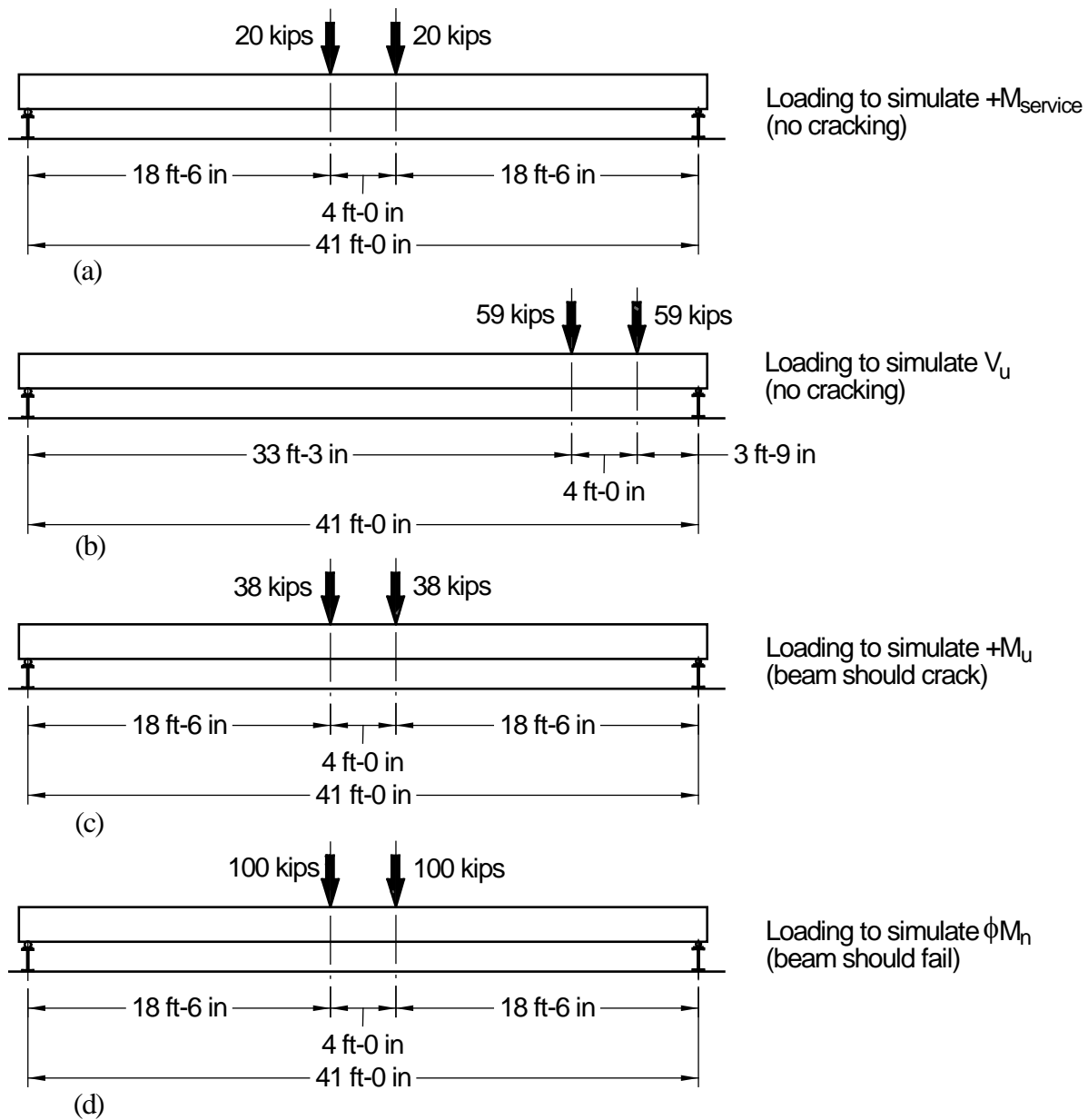


Figure 33. Summary of Loading Arrangements for the Three Tests, (a) Simulation of Service Level Design Positive Moment, (b) Simulation of Strength Level Design Vertical Shear, (c) Simulation of Strength Level Design Positive Moment and Nominal Moment Capacity

load required to simulate strength level design shear was estimated to be 118 kips (59 kips on each tire print). The strength level design vertical shear was simulated on the portion of the composite beam without any extended stirrups for the purpose of subjecting the more critical half of the span to the design vertical shear force. The underlying logic in this approach was that if the half of the span without any extended stirrups could resist the design vertical shear force without incurring any slip, then the other half should be able to at least offer a comparable performance. Even though the actuator load in this test simulated strength level design shear forces, the behavior of the composite beam was expected to be linear-elastic when tested material properties were considered.

During the third test, the loading frame was moved back to the mid-span of the composite beam and the load was increased monotonically to simulate strength level design positive moment and the nominal positive moment capacity (Figure 33(c)).

RESULTS

Investigation of Cross-Sectional Shape and Transverse Connection

The results of the five sub-assembly tests from Phase I are summarized in Table 5. The second column shows the load at first cracking. The third column shows either the actuator load at failure or the capacity of the loading frame, whichever was met first. The fourth column shows the factor of safety against cracking, which is calculated based on Equation 1. In the case of the specimen with the tapered web and embedded plate connection and the trial specimen with the straight web and extended bars, the ultimate load could not be achieved because the capacity of the loading frame was reached before the specimens failed. The last column shows the factor of safety at failure, which is calculated based on Equation 2.

$$FS_{cracking} = \frac{(M_{cracking} + M_{selfweight} + M_{spreaderbeam})}{M_{service}} \quad (1)$$

$$FS_{ultimate} = \frac{(M_{ultimate} + M_{selfweight} + M_{spreaderbeam})}{M_{service}} \quad (2)$$

where

$FS_{cracking}$ = Factor of safety against cracking

$FS_{ultimate}$ = Factor of safety at failure

$M_{cracking}$ = Moment at mid-span due to actuator load at first cracking (P_{cr})

$M_{ultimate}$ = Moment at mid-span due to actuator load at failure (P_u)

$M_{selfweight}$ = Moment at mid-span due to self-weight of specimen

$M_{spreaderbeam}$ = Moment at mid-span due to weight of spreader beam

$M_{service}$ = Moment at service in the transverse direction (based on FEA)

Table 5. Phase I Test Results

Specimen ID	P_{cr} , kips	P_u , kips	FS_{cr}	$FS_{ultimate}$
Trial	80	300 (test stopped due to capacity of the frame)	2.27	7.48
1	90	260 (many cracks in CIP topping in all directions)	2.50	6.53
2	100	225 (fracture of weld at one location and rebar at another)	2.74	5.70
3	110	300 (test stopped due to capacity of the frame)	2.98	7.48
4	60	90 (big crack through precast section)	1.80	2.50

The test results obtained from experimental Phase I are discussed in the following sections, each addressing one aspect of behavior.

Behavior Up to Service Level Loads

Figure 34 shows the load versus vertical mid-span deflection for all five test specimens up to first crack. The service level load determined in the finite element analysis is shown by a

dashed line. It can be seen that all specimens performed similarly. Even the specimen that had a tapered web and no mechanical connection between the precast components and the cast-in-place topping experienced its first crack at a load that was 1.8 times the corresponding service level load.

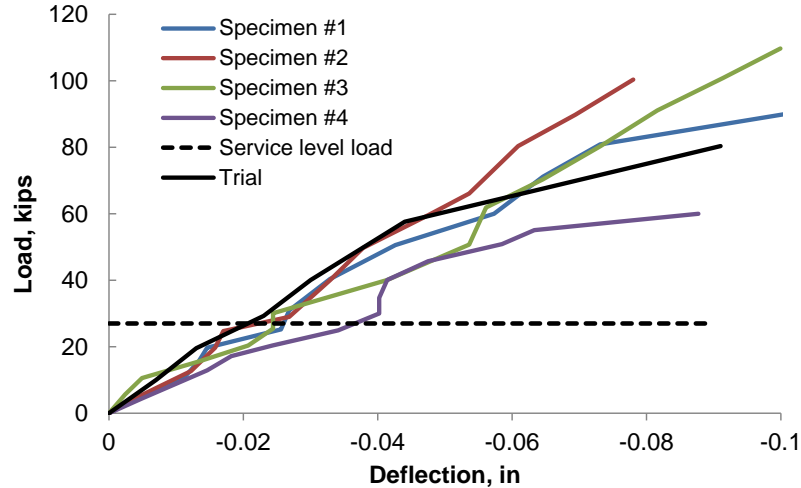


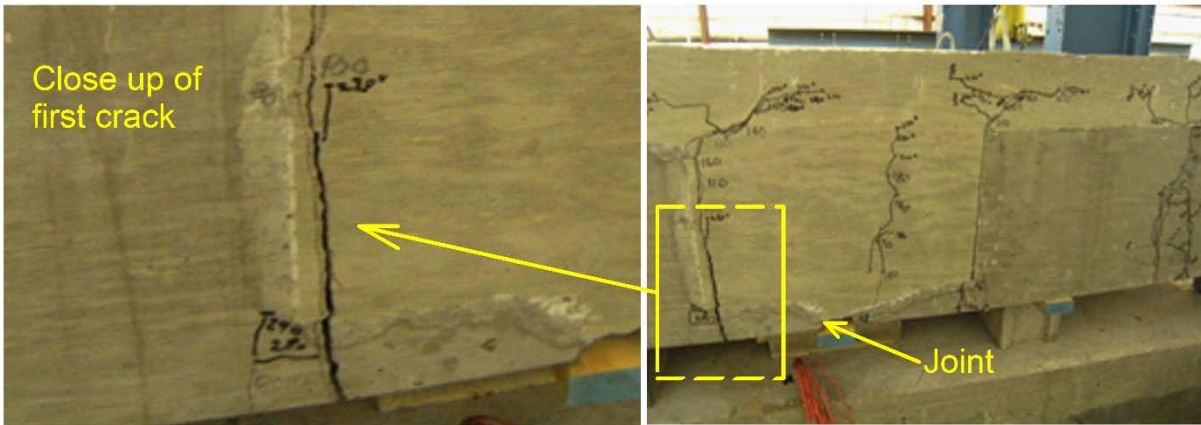
Figure 34. Comparison of Load-Deflection Curves for All Five Specimens to Approximately First Crack

Figure 35 shows the crack patterns of the Trial Specimen and Specimen No. 1 at failure as well as a close-up of the first crack. In both of these specimens, the first crack occurred at the intersection of the precast flange and precast web coupled with a bond failure at the interface between the sides of the precast webs and the cast-in-place topping. The first crack for the Trial Specimen and Specimen No. 1 occurred at 80 kips and 90 kips, respectively. The intersection of the precast flange and web represents a radical change in the geometry of the specimen and is prone to stress concentrations. In addition, weak areas may be created due to lack of proper consolidation of concrete during placement.

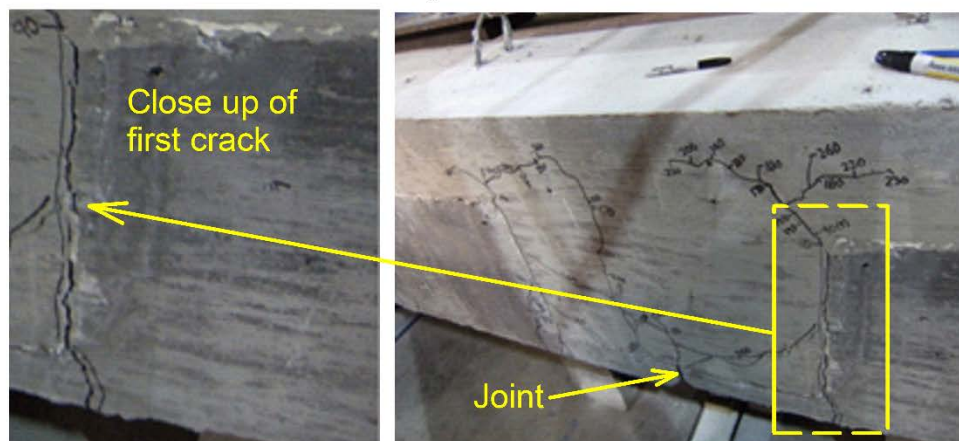
Specimen No. 2 exhibited a similar crack pattern when the first crack occurred. The first crack in Specimen No. 2 occurred at 100 kips. The crack at the intersection of the precast flange and web was associated with a bond failure at the vertical interface between the precast and cast-in-place concretes (Figure 36). Such a location for the first crack was expected because of the presence of welded connections between the tips of the precast flanges.

In Specimen No. 3, first cracking included a crack at the intersection of the precast flange and web, bond failure between the tapered precast web and cast-in-place topping, and another crack in the precast section within the constant moment region (Figure 36). The first crack in Specimen No. 3 occurred at 110 kips.

Finally, in Specimen No. 4, the first crack occurred over the joint between the precast components in the cast-in-place topping (Figure 36). The cast-in-place section over the joint is the most prone to cracking because of the reduction in the cross section due to the presence of the joint. The first crack in Specimen No. 4 occurred at 60 kips.



Trial Specimen



Specimen No. 1

Figure 35. Photographs of Trial Specimen and Specimen No. 1

Behavior Up to Failure

Figure 37 shows the relationship between the load and the vertical deflection at mid-span for all five test specimens up to failure. The specimens with the straight web and the extended bars and the specimen with the tapered web and the embedded plate achieved higher ultimate loads than the other three specimens. However, such a relative comparison is not really useful or practical because the ultimate loads for these two specimens were at least six times the service level load. The presence of damaged flanges in the Trial Specimen did not adversely affect its behavior. In fact, the Trial Specimen was one of the two specimens in which the capacity of the loading frame was met before the specimen failed.

The failure of Specimen No. 2 was caused by the failure of the welded connection between the back of the embedded plate and the transverse bars in the precast flange (Figure 36). This failure is attributed to defects in the welded joint and highlights the importance of creating a connection with a high quality, full penetration weld. However, it is important to note that this failure occurred well past the service level load.

The ultimate failure mode for Specimen No. 4 was a large crack in the precast component at a load equal to 90 kips, which is 2.5 times the equivalent service level load (Figure 36). This

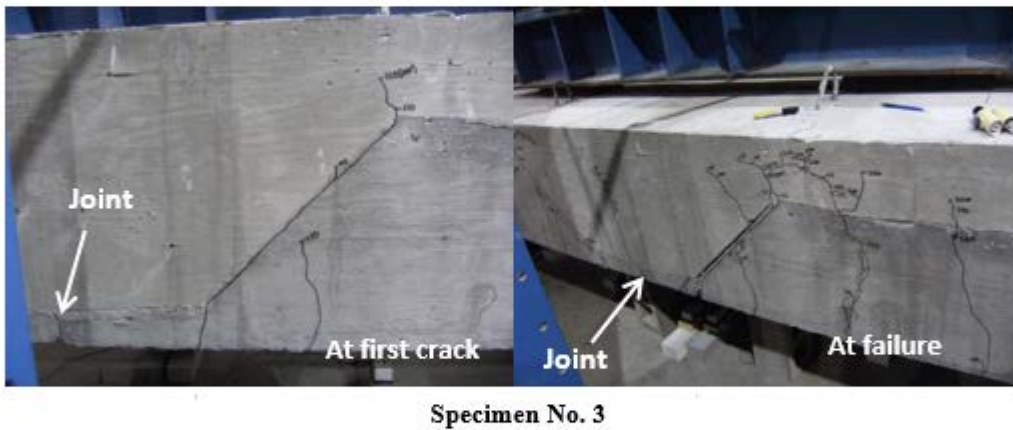
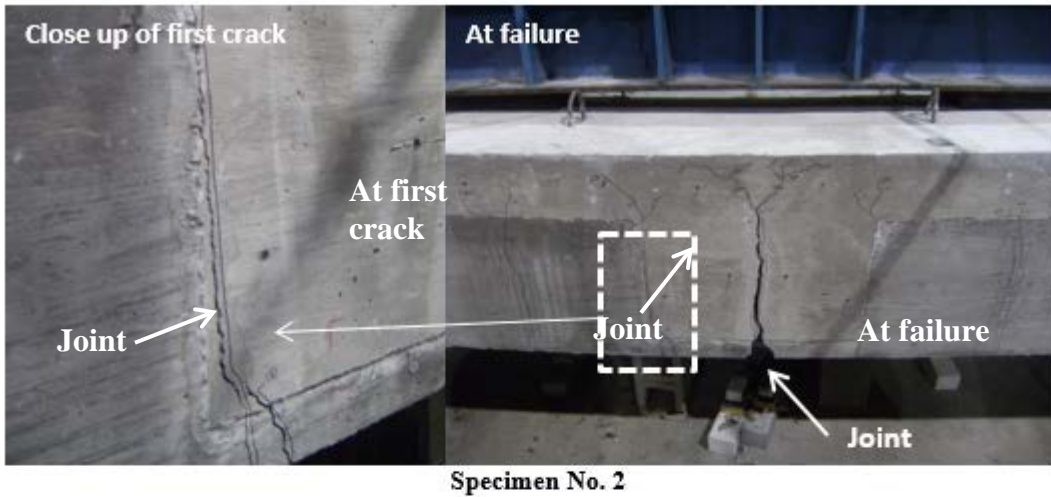


Figure 36. Photographs of Specimen Nos. 2-4

occurred because the transverse reinforcing steel in the precast flanges consisted only of No. 3 bars at 18 in on center, which was less than the bottom transverse steel provided in the cast-in-place topping, which consisted of No. 6 bars at 12 in on center. Therefore, this failure load is expected to improve by increasing the area of transverse steel in the precast flange so that it matches that provided in the cast-in-place topping.

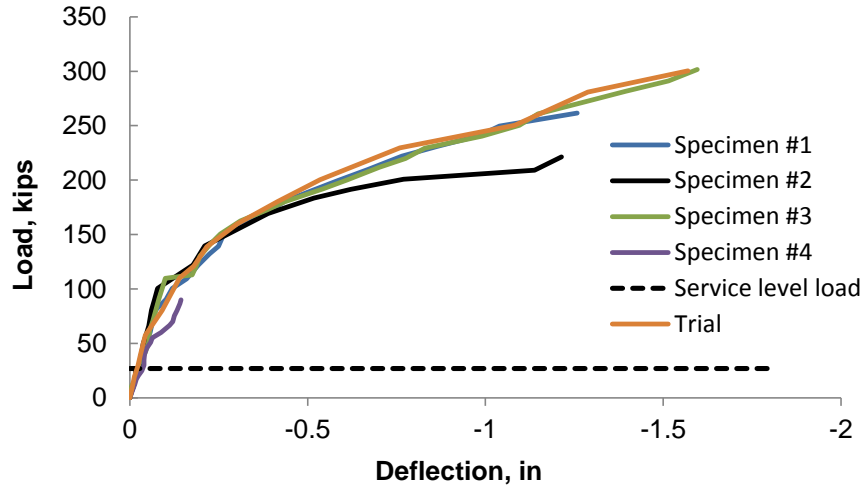


Figure 37. Comparison of Load-Deflection Curves for Phase I Specimens

Simulation of Monolithic Action

Displacement sensors were installed at the bottom of the specimens near the supports at quarter points and at mid-span to obtain the deflected shape of the specimens and to determine whether they would deflect as two rigid bodies hinged at mid-span, where there is a joint between the flanges of the inverted T-beams, or whether they would deflect as one monolithic body. Figure 38 illustrates a typical deflected shape based on the deflections recorded from the displacement sensors. The deflection near the supports is a result of the deformation of the neoprene bearing pads. As can be seen, this deformed shape is closer to the behavior of a monolithic beam than that of two independent rigid bodies. This provides evidence that the inverted T-beam concept can deliver the advantages of jointless, monolithic, cast-in-place concrete construction while saving time in the field by eliminating the need for constructing formwork.

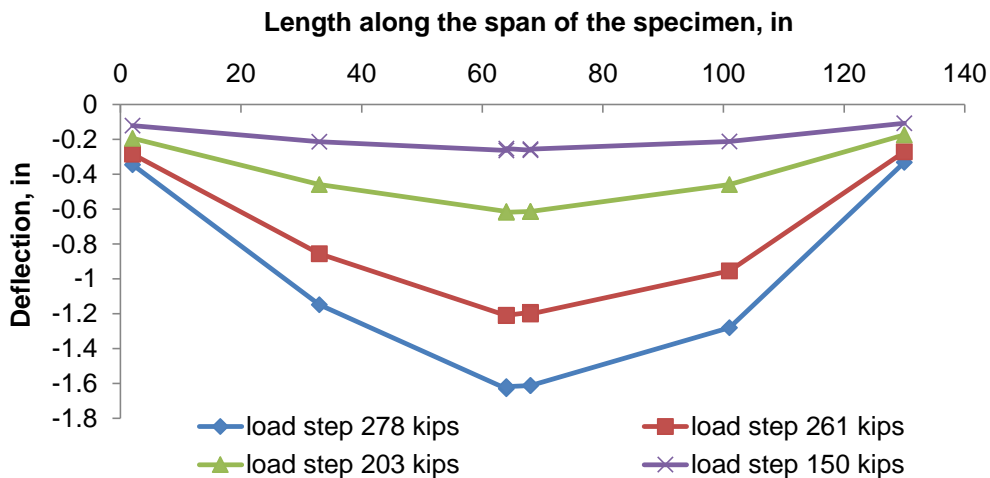


Figure 38. Typical Deflected Shape (Trial Specimen)

Test Results From Experimental Phases I and II

Table 6 provides a summary of the cracking loads and ultimate loads for all tests performed in Experimental Phases I and II. It is important to note that the results from the first seven tests can be compared with each other because the loading arrangement was the same (loading at $\frac{1}{4}$ points).

The last specimen (Specimen No. 7) was subject to a point load offset from the center, as shown in Figure 26, and, therefore, cracking and failure loads cannot be directly compared with the rest of the specimens.

Table 6. Test Results for Phase I and Phase II

Specimen ID	P_{cr} (kips)	P_u (kips)	FS_{cr}	$FS_{ultimate}$
Trial	80	300 (test stopped due to capacity of the frame)	2.27	7.48
1	90	260 (many cracks in CIP topping in all directions)	2.50	6.53
2	100	225 (fracture of weld at one location and rebar at another)	2.74	5.70
3	110	300 (test stopped due to capacity of the frame)	2.98	7.48
4	60	90 (large crack through precast section)	1.80	2.50
5	70	240 (large crack in CIP topping above the joint)	2.00	6.00
6	70	140 (large crack in CIP topping above the joint and parallel with the tapered interface on one side)	2.00	3.70
7	50	81	2.00	3.10

One of the goals of Experimental Phase II was to improve the ultimate strength of the specimen with no mechanical connection by increasing the size of the bars and decreasing their spacing. A comparison of ultimate loads for Specimens No. 4, No. 5 and No. 6 reveals that this goal was achieved. The same conclusion can be drawn by looking at Figure 39, which shows the load-deflection curves for Specimens No. 4, No. 5 and No. 6. It can be seen that Specimens No. 5 and No. 6 performed much better than Specimen No. 4.

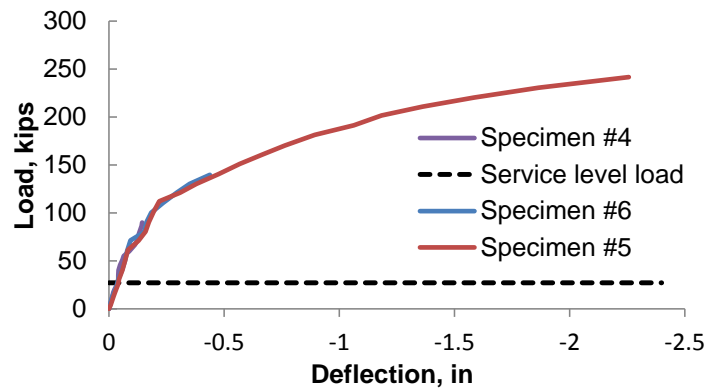


Figure 39. Comparison of Load-Deflection Curves for Specimens with No Mechanical Connection, Tested in Flexure

The cracking loads for these three specimens are similar and the first crack for all three specimens occurred over the joint between the precast flanges. This similarity in behavior up to

the first crack is illustrated in Figure 40. Figure 41 shows the crack patterns at first crack and at failure for all three specimens tested in Phase II. The addition of reinforcing steel in the precast component was expected to prevent a failure mode with a large crack in the precast section, which was observed in Specimen No. 4, even though this failure occurred at a much higher load than the service load. The failure loads for Specimen No. 5 and No. 6 were 140 kips and 240 kips, respectively, compared to a failure load of 90 kips for Specimen No. 4. The difference in the ultimate load for Specimens No. 5 and No. 6 is attributed primarily to the performance of the bond at the interface between the precast and cast-in-place concretes.

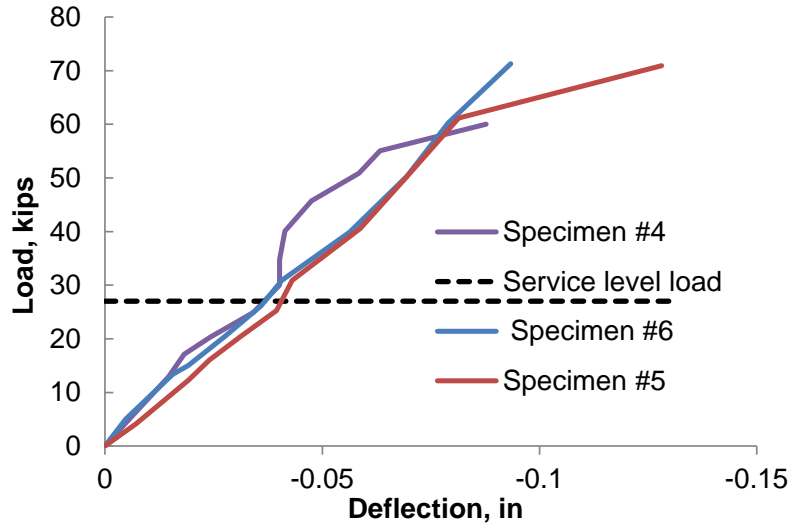
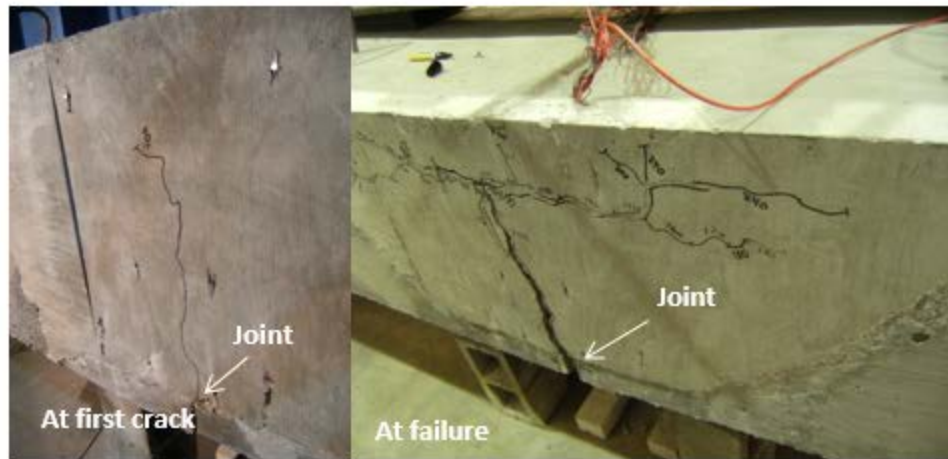
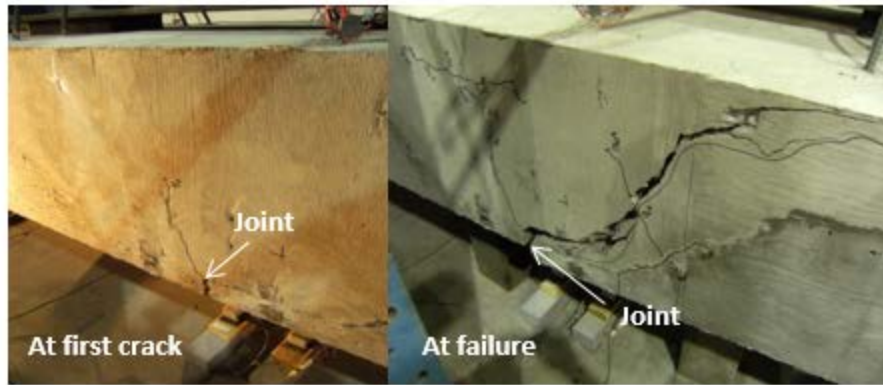


Figure 40. Comparison of Load-Deflection Curves for All Three Specimens Tested in Phase II Up to First Crack

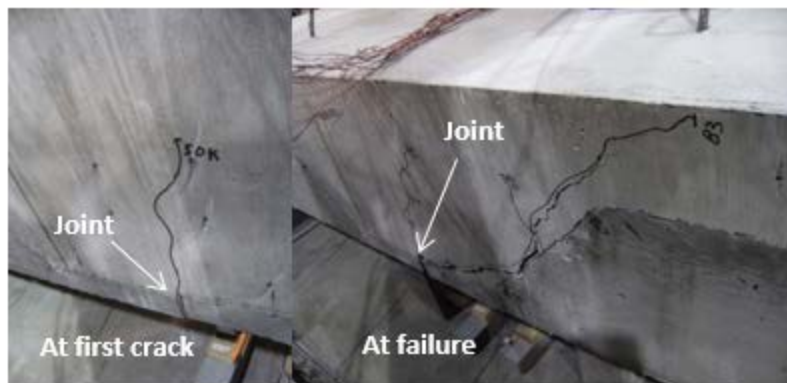
For Specimen No. 5, bond failure started at an actuator load of approximately 120 kips, whereas in Specimen No. 6, the bond performed well almost until failure. This stresses the importance of creating a clean, roughened surface that is free of laitance. During the removal of the grooved wooden formwork, sometimes portions of the corrugations created in concrete would break. This phenomenon was more pronounced in Specimen No. 5. Based on this discussion, it is recommended that the precast fabricator use forms that can deliver the roughened surface while being relatively easy to remove. The use of tighter reinforcement spacing did not correlate to significantly better crack control. Therefore, the No. 6 bars at 12 in on center are favored, as they require less labor for placement. The presence of shear and flexural stresses did not affect the behavior up to the first crack, which occurred at a load twice the service level load. The factor of safety at failure for Specimen No. 7 was 3.1 as opposed to 2.5 for Specimen No. 4. This indicates an improvement as a result of using larger bars and tighter spacing in the precast despite the presence of the shear and flexural stresses. Specimen No. 6, which was subject to pure bending, had a higher factor of safety at failure compared to Specimen No. 7. However, a 20% difference in factors of safety at failure that were at least equal to 3.0 does not represent a concern, even if the joint was subject to a combination of flexural and shear stresses.



Specimen No. 5



Specimen No. 6



Specimen No. 7

Figure 41. Photographs of Specimen Nos. 5-7

Comparison of Transverse Steel to AASHTO Equations

The NCHRP study culminated in recommended design and construction specifications for the inverted T-beam system (French et al., 2011). The design recommendations related to reflective cracking included equations for determining the amount and spacing of transverse load distribution reinforcement and reflective crack control reinforcement. The NCHRP study

recommends that Equation 3 be used to calculate the area of transverse load distribution reinforcement. This equation combines the percentages of longitudinal mild and prestressed flexural reinforcement that need to be provided in the transverse direction based on AASHTO LRFD Bridge Design Specifications equations 5.14.4.1-1 and 5.14.4.1-2, respectively (2013). Because the AASHTO equations were developed for cast-in-place slab systems in which the transverse reinforcement is located immediately above the longitudinal reinforcement, an adjustment is made to account for the fact that the depths to the centers of gravity for the longitudinal prestress and transverse load distribution reinforcement could be significantly different (French et al., 2011). This adjustment is made by multiplying the second part of Equation 3 with α , which is defined below.

$$A_{tld} = k_{mild}A_{l-mild} + \alpha k_{ps}A_{l-ps} \quad (3)$$

$$k_{mild} = \frac{100}{\sqrt{L}} \leq 50\% \quad (4) \text{ (LRFD 5.14.4.1-1)}$$

$$k_{ps} = \frac{100}{\sqrt{L}} \frac{f_{pe}}{60} \leq 50\% \quad (5) \text{ (LRFD 5.14.4.1-2)}$$

where

A_{tld} = area required for transverse load distribution reinforcement, in²

A_{l-mild} = area of longitudinal mild flexural reinforcement, in²

A_{l-ps} = area of longitudinal prestressed flexural reinforcement, in²

k_{mild} = percentage of longitudinal mild flexural reinforcement

k_{ps} = percentage of longitudinal prestressed flexural reinforcement

$\alpha = d_{cgs} / d_{trans} \geq 1.0$

d_{cgs} = depth of center of gravity of prestressed reinforcement, in

d_{trans} = depth of center of gravity of transverse reinforcement, in

L = span length, ft

f_{pe} = effective stress in prestressing strand, ksi.

For the US 360 Bridge, in one 6-ft-wide inverted T-beam, the values are as follows:

$A_{l-mild} = 6 \text{ ea. No. 4 bars} = 1.2 \text{ in}^2$

$A_{l-ps} = 24 \text{ ea. 0.6 in diameter strands} = 5.21 \text{ in}^2$

$L = 43 \text{ ft}$

$f_{pe} = 175 \text{ ksi (assumed)}$

$k_{mild} = \frac{100}{\sqrt{43}} = 15.2\%$

$k_{ps} = \frac{100}{\sqrt{43}} \frac{175}{60} = 44.5\%$

$\alpha = d_{cgs} / d_{trans} \geq 1.0$

$d_{cgs} = 22.5 \text{ in}$

$d_{trans} = 23.5 \text{ in (for welded bar connection)}$

$d_{trans} = 20.5 \text{ in (for non-contact lap splice connection)}$.

Use of these values in Equation 3 provides the area of transverse reinforcement required in 6 ft longitudinally of the bridge, so dividing by 6 will provide the area of transverse steel required per foot length of the bridge. The equation indicates that 0.42 in²/ft is required for the welded connection and 0.45 in²/ft is required for the non-contact lap splice connections. These values are very similar to what was provided in the tested specimens. The welded connection had 2 ea. No. 6 bars in each connection, which were spaced at 2 ft center-to-center, resulting in 0.44 in²/ft. The non-contact lap splice connection specimens had No. 6 bars at 12 in center-to-center (0.44 in²/ft) and No. 4 bars at 6 in center-to-center (0.40 in²/ft), which are both very similar to the reinforcement required by Equation 3.

Results of Deck Mixture Optimization Study

Short-Term Properties

The short-term properties for all seven mixtures are provided in Table 7, Table 8, and Table 9. Experimental data for tensile strength and modulus of elasticity are compared to the values obtained using the equations in the AASHTO LRFD Bridge Design Specifications (2013). These equations are provided in AASHTO Section 5.4.2.4 and Section 5.4.2.6-7, respectively. When cracking is caused by the effects of flexure, AASHTO provides a series of equations for the determination of modulus of rupture (f_r) for both normal-weight and lightweight concrete. These values vary between $0.20\sqrt{f'_c}$ to $0.24\sqrt{f'_c}$ for normal-weight concrete and between $0.17\sqrt{f'_c}$ to $0.20\sqrt{f'_c}$ for lightweight concrete. The commentary of Section C5.4.2.6 states that data show that most modulus of rupture values are between $0.24\sqrt{f'_c}$ and $0.37\sqrt{f'_c}$ (for f'_c in ksi). In addition, the commentary of Section C5.4.2.7 states that the given values may be unconservative for tensile cracking caused by restrained shrinkage, anchor zone splitting, and other similar tensile forces caused by effects other than flexure and that the direct tensile strength stress (f_t) should be used in these cases. Equation 6 is taken from the commentary of Section 5.4.2.7 –Tensile Strength and may be used for normal-weight concrete with specified compressive strengths up to 10 ksi.

Table 7. Compressive Strength Test Results

Age, days	Compressive Strength (psi)						
	NWC-FA	NWC-SL1	SLWC-FA	SLWC-SL	NWC-SLWF-SL	NWC-SL2	NWC-SLWF
7	3,100	3,580	2,600	4,020	3,660	4,080	2,650
14	3,530	nm	3,790	5,270	4,130	4,830	3,280
28	4,260	5,200	4,600	5,950	4,560	5,370	3,540
56	4,140	5,250	4,910	6,420	nm	5,410	3,610
90	4,060	5,410	4,880	6,440	nm	nm	nm

nm = not measured.

Because the focus of this study is potential cracking due to restrained differential shrinkage, Equation 6 is used to compare calculated and tested tensile strength values. Equation 7 is used to calculate the tensile strength of mixtures that contained lightweight coarse aggregates and normal-weight fine aggregates (sand-lightweight). There is no equation in AASHTO that is applicable to the mixtures that contained normal-weight coarse aggregates and a mixture of normal-weight and lightweight fine aggregates. Because the normal-weight aggregates

Table 8. Tensile Strength Test Results Compared to Estimates

Age, days	Tensile Strength (psi)					
	NWC-FA			NWC-SL1		
	Tested	Eq. 6	Tested/(Eq. 6)	Tested	Eq. 6	Tested/(Eq. 6)
7	317	405	0.78	391	435	0.90
28	418	475	0.88	455	524	0.87
90	412	463	0.89	541	535	1.01
			Avg. = 0.85			Avg. = 0.93
	SLWC-FA			SLWC-SL		
	Tested	Eq. 7	Tested/(Eq. 7)	Tested	Eq. 7	Tested/(Eq. 7)
7	274	322	0.85	374	401	0.93
28	370	429	0.86	391	488	0.80
90	435	442	0.98	503	508	0.99
			Avg. = 0.90			Avg. = 0.91
	NWC-SLWF-SL			NWC-SL2		
	Tested	Eq. 6	Tested/(Eq. 6)	Tested	Eq. 6	Tested/(Eq. 6)
7	377	440	0.86	417	470	0.89
28	370	470	0.79	483	510	0.95
90	nm	nc	nc	nm	nc	nc
			Avg. =0.83			Avg. = 0.92
	NWC-SLWF			Summary of Tested Values (28 days), f_t (psi)		
	Tested	Eq. 6	Tested/(Eq. 6)	NWC-FA		418
7	287	370	0.78	NWC-SL1		455
28	340	420	0.81	SLWC-FA		370
90	nm	nc	nc	SLWC-SL		391
			Avg. = 0.80	NWC-SLWF-SL		370
nm=not measured				NWC-SL2		483
nc=not calculated				NWC-SLWF		340

$$f_t = 0.23\sqrt{f'_c} \text{ where } f'_c \text{ is in ksi} \quad (6)$$

$$f_t = 0.20\sqrt{f'_c} \text{ where } f'_c \text{ is in ksi} \quad (7)$$

represented the majority of aggregates in these mixtures, Equation 7 was used for comparison with tested values. However, as can be seen from the results in Table 8, Equation 7 overestimated the tensile strength of the two mixtures that contained a blend of normal-weight and lightweight aggregates. In the calculation of concrete tensile strength using Equations 6 and 7, the tested values were used for the compressive strength of concrete. Although in general, AASHTO's equations overestimated the tensile strength of the investigated mixtures, they provided reasonably good estimates for design purposes. The tensile strength of concrete is an important short-term property because the likelihood of cracking is estimated by comparing the magnitude of tensile stresses created by differential shrinkage with the tensile strength of the cast-in-place concrete deck. Table 8 provides a summary of the tested tensile strength of the seven concrete mixtures at 28 days. The mixture with the lowest tensile strength was the one with normal-weight coarse aggregates and saturated lightweight fines. The mixture with the highest tensile strength was the mixture with normal-weight coarse aggregates and slag, denoted (NWC-SL2).

Table 9. Modulus of Elasticity Test Results Compared to Estimates

Age (days)	Modulus of Elasticity, ksi					
	NWC-FA			NWC-SL1		
	Tested	Eq. 8	Tested/Eq. 8	Tested	Eq. 8	Tested/Eq. 8
7	4,530	3,220	1.41	4,760	3,350	1.42
14	4,280	3,430	1.25	nm	nc	nc
28	4,430	3,770	1.18	5,010	4,040	1.24
56	4,150	3,720	1.12	5,180	4,060	1.28
90	4,360	3,680	1.18	4,730	4,120	1.15
			Avg. = 1.23			Avg. = 1.27
	SLWC-FA			SLWC-SL		
	Tested	Eq. 8	Tested/Eq. 8	Tested	Eq. 8	Tested/Eq. 8
7	2,620	2,230	1.17	2,780	2,690	1.03
14	3,180	2,680	1.19	3,160	3,080	1.03
28	3,080	2,970	1.04	3,540	3,270	1.08
56	3,460	3,070	1.13	3,260	3,390	0.96
90	2,950	3,060	0.96	3,010	3,400	0.89
			Avg. = 1.10			Avg. = 1.00
	NWC-SLWF-SL			NWC-SL2		
	Tested	Eq. 8	Tested/Eq. 8	Tested	Eq. 8	Tested/Eq. 8
7	3,700	3,200	1.16	4,840	3,720	1.30
14	3,390	3,400	1.00	4,960	4,050	1.23
28	4,160	3,570	1.17	5,460	4,270	1.28
56	nm	nc	nc	4,950	4,280	1.16
90	nm	nc	nc	nm	nc	nc
			Avg. = 1.11			Avg. = 1.24
	NWC-SLWF			Summary of Tested Values, E, ksi		
	Tested	Eq. 8	Tested/Eq. 8	NWC-FA		4,430
7	3,510	2,720	1.29	NWC-SL1		5,010
14	4,295	3,030	1.42	SLWC-FA		3,080
28	3,990	3,150	1.27	SLWC-SL		3,540
56	4,670	3,180	1.47	NWC-SLWF-SL		4,160
90	nm	nc	nc	NWC-SL2		5,460
			Avg. = 1.36	NWC-SLWF		3,990

nm = not measured; nc = not calculated.

Tested values for modulus of elasticity of the seven mixtures were compared with those calculated using Equation 8 from AASHTO (2013). Tested unit weight and compressive strength values were used in the evaluation of Equation 8. In general, Equation 8 underestimated the modulus of elasticity of the seven investigated mixtures; however, it provided reasonable estimates for design purposes. Modulus of elasticity is another short-term property that plays an important role in the evaluation of composite bridge systems for the effects of differential shrinkage. Because the quantification of stresses caused by differential shrinkage can be based on the age-adjusted effective modulus method, a higher modulus of elasticity for the deck leads to higher tensile stresses in the deck. Conversely, a lower modulus of elasticity for the deck leads to a lower age-adjusted effective modulus and represents a mixture that can alleviate the tensile stresses in the deck created as a result of differential shrinkage. In addition, the modulus of elasticity of concrete increases with time; this is why the age-adjusted effective modulus method uses an aging coefficient that accounts for this effect. Such an increase in the modulus of elasticity works against the concept of alleviating tensile stresses that result from differential

shrinkage because it makes the concrete stiffer and less accommodating toward restrained deformations.

$$E_c = 33,000 K_1 w_c^{1.5} \sqrt{f'_c} , \text{ where } w_c \text{ is in k/ft}^3 \text{ and } f'_c \text{ is in ksi} \quad (8)$$

Table 9 provides a summary of the moduli of elasticity for the seven mixtures at 28 days. The mixture with the lowest modulus of elasticity is the mixture with saturated lightweight coarse aggregates and fly ash. The mixture with the highest modulus of elasticity is the one with normal-weight coarse aggregates and slag, denoted (NWC-SL2). The comparison of tensile strength and modulus of elasticity for the seven mixtures illustrates how difficult it is to find a mixture that embodies all the desired properties. For example, the mixture denoted NWC-SL2 had the highest tensile strength, but also had the highest modulus of elasticity.

Long-Term Properties

Figure 42 shows the development with time of drying shrinkage strains for the seven mixtures investigated. In this report, shortening strains are positive. Because the changes in shrinkage strains recorded after 70 days were generally negligible, shrinkage testing was stopped at 100 days. It is important to note that the measured shrinkage strains represent primarily drying shrinkage strains. Shrinkage specimens were moist-cured for 7 days and were then exposed to drying at relative humidity of $50 \pm 4\%$ per ASTM C157. Table 10 provides a summary of the shrinkage strains at 100 days. The mixture with the lowest shrinkage was the mixture with normal-weight coarse aggregates and saturated lightweight fine aggregates. The mixture with the highest shrinkage was the mixture with saturated lightweight coarse aggregates and slag. The two mixtures that contained saturated lightweight coarse aggregates exhibited the highest shrinkage strains.

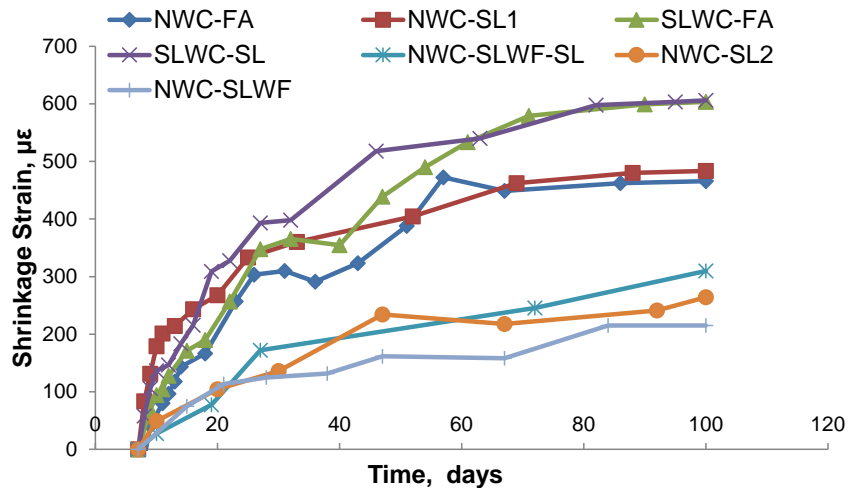


Figure 42. Experimental Data on Shrinkage Strain Versus Time (Unrestrained Shrinkage Test)

Table 10. Summary of Experimental Shrinkage Strains at 100 Days

Mixture	Shrinkage Strains at 100 Days, $\mu\epsilon$
NWC-FA	466
NWC-SL1	483
SLWC-FA	603
SLWC-SL	606
NWC-SLWF-SL	310
NWC-SL2	264
NWC-SLWF	215

Figure 43 shows the development with time of measured strains during the creep test. Figure 43(a) shows the total strain, which is defined in Equation 9 as the summation of elastic strain, shrinkage strain and creep strain. Elastic strain is the strain measured immediately after the creep specimens are loaded. Shrinkage strain is the strain due to the shrinkage of the creep specimens during the creep tests and is measured from unloaded companion cylinders. Creep strain is the increase in strain in the creep specimens over time as a result of the applied load.

$$\text{total strain} = \text{elastic strain} + \text{shrinkage strain} + \text{creep strain} \quad (9)$$

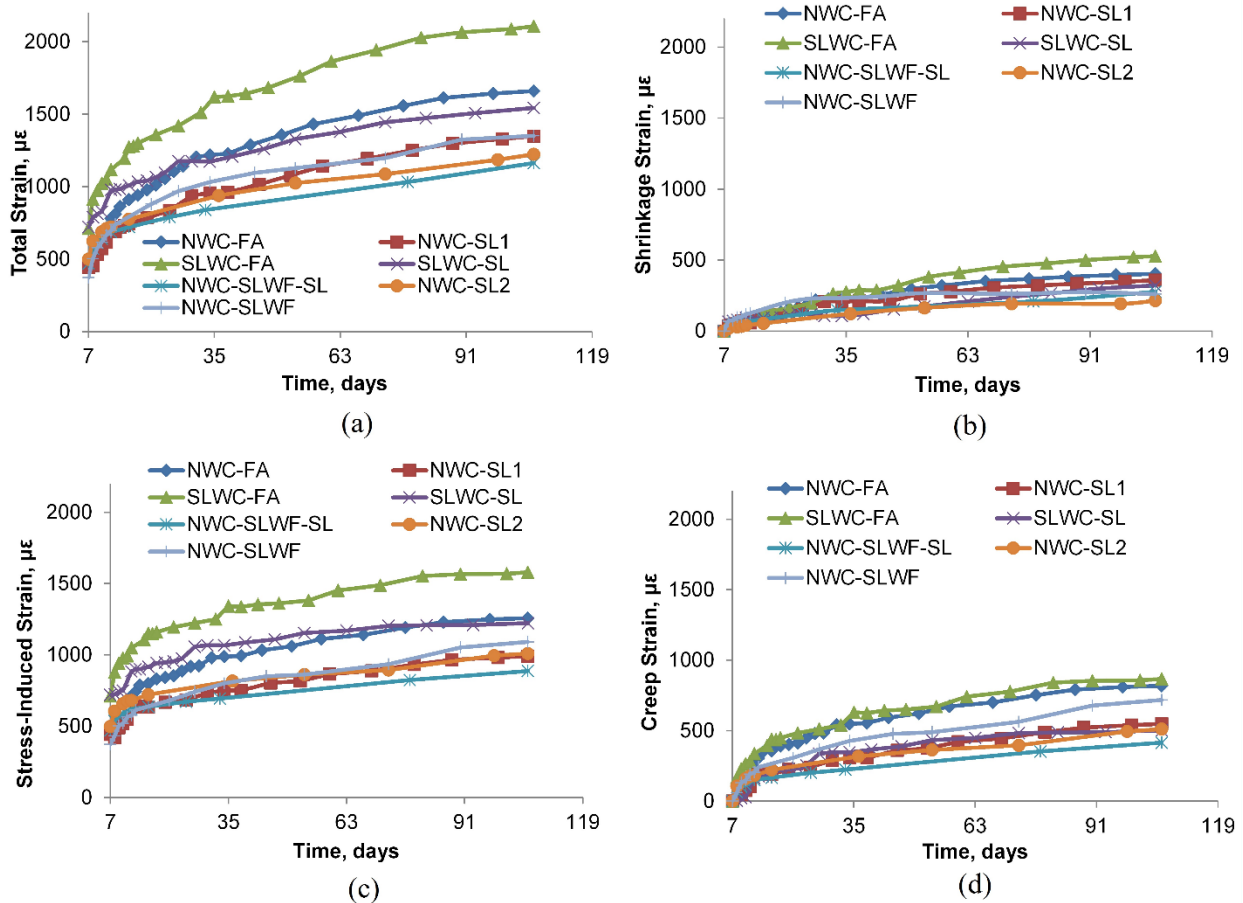


Figure 43. Creep Test Results, (a) Total Strain, (b) Shrinkage Strain, (c) Stress-Induced Strain, (d) Creep Strain

Because the change in total strains recorded from the creep test after 80 days were negligible, creep tests were terminated at 106 days. Figure 43(b) shows the shrinkage strain measured in the unloaded companion specimens, which was deducted from the total strain to obtain the stress-induced strain. Figure 43(c) shows the stress-induced strain, which is defined in Equation 10. Stress-induced strain is the strain caused only by the sustained load (or sustained stress) over time and can be expressed as the summation of the elastic strain and creep strain. Alternatively, stress-induced strain can be expressed as the total strain measured in the creep specimens minus the shrinkage strain measured in unloaded companion cylinders.

$$\begin{aligned} \text{stress induced strain} &= \text{elastic strain} + \text{creep strain} && \text{or} && (10) \\ \text{stress induced strain} &= \text{total strain} - \text{shrinkage strain} \end{aligned}$$

Figure 43(d) shows the creep strain. Creep strain was obtained by deducting the elastic strain from the stress-induced strain. One of the parameters used in the analysis for time-dependent effects is the creep coefficient. Creep coefficient is the ratio of creep strain to the initial elastic strain (Equation 11). A plot of the creep coefficient versus time is presented in Figure 44.

$$\text{creep coefficient} = \frac{\text{drying creep strain}}{\text{initial elastic strain}} \quad (11)$$

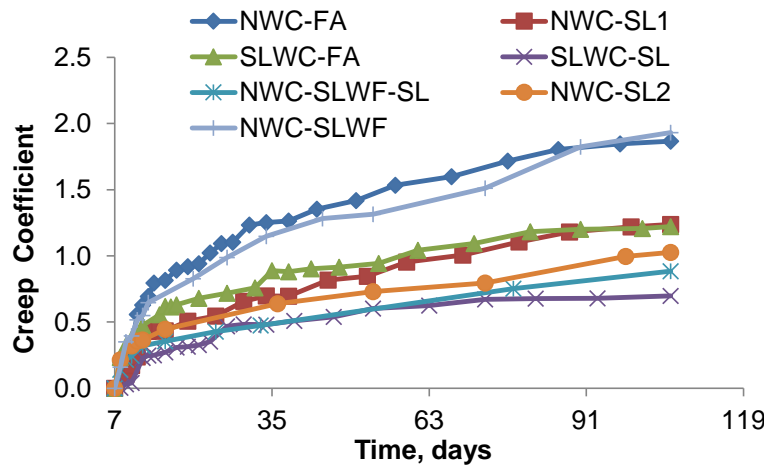


Figure 44. Creep Coefficient vs. Time

Table 11 provides a summary of the experimental data from creep tests. Elastic strains for the two mixtures containing saturated lightweight coarse aggregates are higher than the rest of the mixtures. This is expected because lightweight mixtures typically have lower moduli of elasticity compared to normal-weight mixtures (as shown in Table 9). There were several differences between the shrinkage strains measured during the shrinkage tests and those measured from the unloaded companion cylinders during the creep tests. For example, the NWC-SLWF, NWC-SL2 and NWC-SLWC-SL mixtures exhibited the lowest shrinkage strains compared to the other mixtures. However, the lowest shrinkage strain in the creep tests was measured in the NWC-SL2 mixtures as opposed to the NWC-SLWF mixture. Shrinkage strains measured during the creep test in the NWC-FA, NWC-SL1, SLWC-FA and SLWC-SL were also not entirely consistent with those measured from the shrinkage prisms. The highest disparity

was observed in the shrinkage measurements for the SLWC-SL mixture. During the creep tests, this mixture exhibited the lowest shrinkage strain compared to NWC-FA, NWC-SL1 and SLWC-FA mixes, whereas the data from the shrinkage prisms revealed the opposite.

Table 11. Summary of Experimental Data From the Creep Tests

Type of Strain	NWC-FA	NWC-SL1	SLWC-FA	SLWC-SL	NWC-SLWF-SL	NWC-SL2	NWC-SLWF
Elastic strain ($\mu\epsilon$)	439	442	711	720	470	498	372
Shrinkage strain ($\mu\epsilon$)	402	358	527	321	276	214	260
Creep strain ($\mu\epsilon$)	819	548	868	502	416	511	719
Total strain ($\mu\epsilon$)	1,660	1,348	2,106	1,543	1,162	1,223	1,351
Creep Coefficient	1.87	1.24	1.22	0.70	0.89	1.03	1.93

Because creep strain is calculated by subtracting elastic and shrinkage strains from the total strain, the magnitudes of the elastic and shrinkage strains play an important role in this determination. In this study, creep coefficient is used as the metric for comparing creep properties of the seven mixtures, because this coefficient is employed in the age-adjusted effective modulus method.

Table 12 provides a summary of the long terms properties of the seven investigated mixtures. The NWC-SLWF mixture exhibited the lowest shrinkage, whereas the SLWC-SL mixture exhibited the highest. The NWC-SLWF mixture also exhibited the highest creep coefficient, whereas the SLWC-SL mixture exhibited the lowest creep coefficient. While it may be typically difficult to find a mixture that exhibits both low shrinkage and high creep properties, in this study the NWC-SLWF mixture possessed both of these characteristics and is considered a desirable mixture, whereas the SLWC-SL mixture is considered an undesirable one. It should be noted that since the NWC-SLWF mixture does not have a supplemental cementitious material, it may not have acceptably low permeability. For other situations where the combination of low shrinkage and high creep may not be possible, priority should be given the mixture with the lowest shrinkage because it is the free shrinkage of the deck that serves as a catalyst for the creation of tensile stresses in the cast-in-place topping and potentially excessive cracking. In addition, sensitivity studies can be performed for a given structure to determine the influence of the short and long term properties of the concrete materials on the structural effects of shrinkage and creep.

Table 12. Summary of Experimental Data on Shrinkage and Creep Properties (100 Days)

Mixture	Drying Shrinkage Strain ($\mu\epsilon$)	Creep Coefficient
NWC-FA	466	1.87
NWC-SL1	483	1.24
SLWC-FA	603	1.22
SLWC-SL	606	0.70
NWC-SLWF-SL	310	0.89
NWC-SL2	264	1.03
NWC-SLWF	215	1.93

Results of Composite Action Study

Analytical Investigation

Before the three tests were conducted, an estimation of the vertical and horizontal shear capacity of the composite beam was performed based on AASHTO LRFD Design Specifications (2013) using several assumptions. These estimations were conducted to ensure that the composite beam had adequate vertical and horizontal shear strength to resist the loads induced during the three tests. In addition, an estimation of the actuator load versus mid-span deflection curve was estimated assuming full composite action, with the purpose of comparing this curve with the one obtained experimentally.

Estimation of Vertical Shear Capacity

The estimation of the vertical shear capacity was performed in accordance with Article 5.8.3.3 of AASHTO LRFD Design Specifications (2013) based on Equations 12, 13, and 14. In addition, the vertical shear strength provided by concrete was calculated using the entire composite cross section and the lower concrete compressive strength ($f'_c = 4$ ksi). Furthermore, this estimation was conservatively based on the simplified procedure for non-prestressed sections. Vertical stirrups were considered to provide shear strength only if they were extended in the cast-in-place topping. The bent transverse bars in the cast-in-place topping and the closed stirrups that enclose the prestressing strands in the precast beam were considered to contribute toward the vertical shear resistance of the composite section. Vertical shear demand was calculated at the critical section and was based on the loads simulated during Test 2. This information is provided in Table 13. The last column in Table 13 gives the ratio of the vertical shear demand to the vertical shear capacity. It can be observed that, even when the contribution of the extended stirrups is ignored, the demand-to-capacity ratio is still considerably lower than unity.

$$V_n = \min \begin{cases} V_c + V_s + V_p \\ 0.25 f'_c b_v d_v + V_p \end{cases} \quad (12)$$

$$V_c = 0.0316\beta\sqrt{f'_c} b_v d_v \quad (13)$$

$$V_s = \frac{A_v f_y d_v (\cot\theta + \cot\alpha) \sin\alpha}{s} \quad (14)$$

Table 13. Calculated Vertical Shear Demand and Vertical Shear Strength

Portion of Beam	Vertical Shear Strength, kips				$\phi V_n = \phi V_c + \phi V_s$	Vertical Shear Demand V_u , kips	Ratio $V_u / \phi V_n$
	ϕV_c	ϕV_s					
		$\phi V_{s, \text{extended}}$	$\phi V_{s, \text{inclined PC}}$	$\phi V_{s, \text{bent CIP}}$			
without extended stirrups	168	0	82	62	312	138	0.44
with extended stirrups	168	82	82	62	394	138	0.35

ϕ =resistance factor; V_u =Ultimate factored shear load, V_c = shear strength of concrete, $V_{s, \text{extended}}$ = shear strength of extended stirrups, $V_{s, \text{inclined PC}}$ = shear strength of the inclined stirrups in the precast concrete, $V_{s, \text{bent CIP}}$ = shear strength of the bent bars in the cast-in-place topping, V_s = sum of shear strength of all reinforcement, V_n = nominal shear strength.

Estimation of Horizontal Shear Demand and Capacity

To ensure full composite action, the interface shear force must be smaller than the horizontal shear strength of the interface. There are various ways to calculate the interface shear force, or horizontal shear demand. When a beam is uncracked and its behavior is linear-elastic, horizontal shear stresses can be estimated using the following equation:

$$v_h = \frac{VQ}{Ib_v} \quad (15)$$

where

V = vertical shear force at location under consideration

Q = first moment of area of portion above interface with respect to neutral axis

I = moment of inertia of composite cross section

b_v = width of the interface.

Loov and Patnaik (1994) state that this equation can be used to evaluate the horizontal shear stress for cracked beams if Q and I are based on the cracked section. Because it provides a common basis for comparison, this equation was adopted in previous studies, even though Hanson (1960) and Saeman and Washa (1964) recognized that it does not give an exact representation of the horizontal shear stress at failure. As an alternative to the classical elastic strength of materials approach, a reasonable approximation of the factored interface shear force at the strength or extreme event limit state for either elastic or inelastic behavior and cracked or uncracked sections can be provided by Equations 16 and 17 (AASHTO, 2013).

$$V_{ui} = v_{ui}A_{cv} \quad (16)$$

where

V_{ui} = factored interface shear force on area A_{cv} , kips

v_{ui} = factored interface shear stress, ksi

A_{cv} = area of concrete considered to be engaged in horizontal shear transfer, in².

$$v_{ui} = \frac{V_u}{b_{vi}d_v} \quad (17)$$

where

V_u = factored vertical shear force at section under consideration, kips

b_{vi} = interface width considered to be engaged in shear transfer, in

d_v = the distance between the centroid of the tension steel and the mid-thickness of the slab to compute a factored interface shear stress, in.

The interface shear force can also be calculated based on equilibrium conditions by computing the actual change in compressive or tensile force in any segment (ACI 318, 2014). For example, if the change in the compressive force over a segment of length l_v is C , and if the

width of the interface is b_v , then the horizontal shear stress can be computed by Equation 18, which implies that the entire length of the shear span can be used to transfer the horizontal shear force:

$$v_{ui} = \frac{c}{b_v l_v} \quad (18)$$

where

c = change in the compressive force over a segment of length l_v , kips.

To determine whether slip could be prevented, a comparison of the horizontal shear demand and capacity was performed. Horizontal shear demand was based on the loads simulated during Test 2 and was determined using Equations 15, 17, and 18 (Table 14). Because the composite beam remained uncracked during Test 2, the utilization of Equation 15 using transformed uncracked section properties was appropriate.

Table 14. Horizontal Shear Stress (Test 2 – Simulation of Strength Level Design Shear)

Eq.	Horizontal Shear Stress, psi		
	Plane 1	Plane 2	Plane 3
15	99	65	Varies
17	96	96	NA
18	46	46	40

NA = not applicable.

Three possible failure planes were examined for the inverted T-beam as shown in Figure 45. Plane 1 consists of the interface between the top of the precast web and the cast-in-place topping plus the rest of the width of the composite section. Plane 1 includes an intentionally roughened interface in the transverse direction and monolithic planes. Plane 2 consists of the interfaces between the precast flanges and cast-in-place topping and the bottom width of the precast beam web. Plane 2 includes intentionally roughened interfaces in the longitudinal direction and a monolithic plane. Plane 3 consists of the entire interface between the precast and cast-in-place components and includes roughened interfaces in the transverse and longitudinal directions.

Equation 15 yields higher horizontal shear stresses in Plane 1 compared to Plane 2 because Plane 1 is closer to the neutral axis, which is where horizontal shear stresses are highest in an un-cracked section. A single horizontal shear stress value for Plane 3 could not be calculated using Equation 15 because Plane 3 consists of sub-planes whose distances to the neutral axis vary. Equation 17, yielded a similar horizontal shear stress value as that calculated for Plane 1 using Equation 15, which confirms that it provides a reasonable approximation of the horizontal shear stress. An examination of the derivation of Equation 17 reveals that this equation does not differentiate between horizontal shear stresses in any horizontal plane between the internal compression and tension forces. Also, because Equation 17 is a reasonable approximation for calculating horizontal shear stresses in *horizontal* planes, it does not apply to Plane 3. For the loading arrangement illustrated in Test 2, Equation 18 yields the average horizontal shear stress between the point of maximum moment and the point of zero moment.

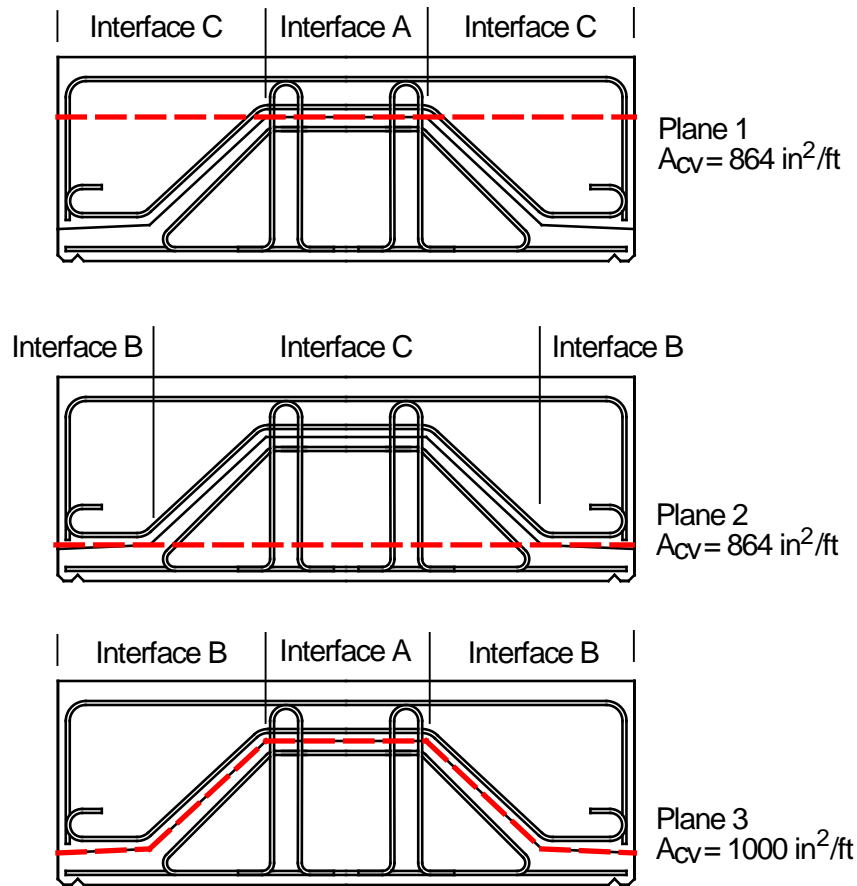


Figure 45. Potential Failure Planes Due to Horizontal Shear

Because the shear diagram between these two points is not constant, the horizontal shear stress calculated using Equation 18 is lower than that calculated using either Equation 15 or 17, which capture the maximum horizontal shear stress or an approximation of it.

Horizontal shear capacity was calculated based on AASHTO LRFD Specifications (2013) (Equation 19). In the estimation of the horizontal shear capacity, three potential slip planes were considered (Figure 45). The horizontal shear capacity for each plane was calculated by using the appropriate cohesion and friction factors for the types of interfaces that comprised each plane (monolithic, roughened or not roughened). The cohesion and friction factors for the assumed interface conditions are provided in Table 15.

$$V_{ni} = cA_{cv} + \mu (A_{vf}f_y + P_c) \leq \min \left\{ \begin{array}{l} K_1 f'_c A_{cv} \\ K_2 A_{cv} \end{array} \right. \quad (19)$$

Table 15. AASHTO LRFD Specification Cohesion and Friction Factors

Value	Interface A (Intentionally roughened)	Interface B (Not intentionally roughened)	Interface C (monolithic)
Cohesion (c)	0.28	0.075	0.40
Friction (μ)	1	0.6	1.4
K_1	0.3	0.2	0.25
K_2	1.8	0.8	1.5

In addition, the estimation of the horizontal shear capacity was performed by both accounting for the presence of the extended stirrups and ignoring them. The results of this estimation are provided in Table 16. The horizontal shear demand and capacity values provided in Table 16 were calculated for 1 ft of length. The horizontal shear demand in terms of force was calculated by multiplying the horizontal shear stress values in Table 15 by the corresponding interface areas. The last six columns show the ratio between the horizontal shear demand and capacity and suggest that a horizontal shear failure should not occur. As stated earlier, one of the goals of this study was to investigate experimentally whether adequate horizontal shear strength in such a uniquely shaped composite member can be provided solely by the natural cohesion between the two components.

Table 16. Comparison of Estimated Design Horizontal Shear Force and Horizontal Shear Capacity

Eq.	Demand (kips) (per foot of length)			Capacity (kips) (per foot of length)						Ratio, Demand/Capacity					
	Plane 1	Plane 2	Plane 3	Plane 1		Plane 2		Plane 3		Plane 1		Plane 2		Plane 3	
				St.	N.S.	St.	N.S.	St.	N.S.	St.	N.S.	St.	N.S.	St.	N.S.
15	86	56	Varies	493	317	368	256	204	124	0.17	0.27	0.15	0.22	Varies	
17	83	83	NA	493	317	368	256	204	124	0.17	0.26	0.23	0.32	NA	
18	46	46	40	493	317	368	256	204	124	0.09	0.15	0.13	0.18	0.2	0.32

St. = with stirrups, N.S. = without stirrups, NA=not applicable.

Estimation of Full Load Versus Mid-Span Displacement Curve

To verify full composite action behavior of the system under various stages of loading, the full anticipated load versus mid-span deflection curve of the simply supported beam system was estimated analytically for comparison with the load versus mid-span deflection curve obtained experimentally. To do this, material models defining the stress-strain relationships for the two types of concrete and the prestressing steel present in the composite system had to be adopted.

Stress-Strain Relationship

For the precast and CIP concrete materials, the Hognestad model (1951) was adopted and calibrated to match the tested compressive strength at 28 days. The design compressive strengths for the precast and cast-in-place components were $f'_c = 6$ ksi and $f'_c = 4$ ksi, respectively. The tested compressive strengths for the precast and cast-in-place components were 10.2 ksi and 8.5 ksi, respectively. The model consists of a second-degree parabola with apex at strain ϵ_0 , which is the strain when f_c reaches f'_c . In this case, ϵ_0 was taken equal to 0.0025. This model is described mathematically in Equation 20 and graphically in Figure 46. The maximum usable concrete strain was taken equal to 0.004. This model is convenient for use in analytical studies involving concrete because the entire stress-strain curve is given by one continuous function. The material model for the prestressing steel consisted of a tri-linear curve, which is mathematically described by the piecewise functions in Equation 21 and illustrated in Figure 47.

$$f_c = f'_c \left[\frac{2\epsilon_c}{\epsilon_0} - \left(\frac{\epsilon_c}{\epsilon_0} \right)^2 \right] \quad (20)$$

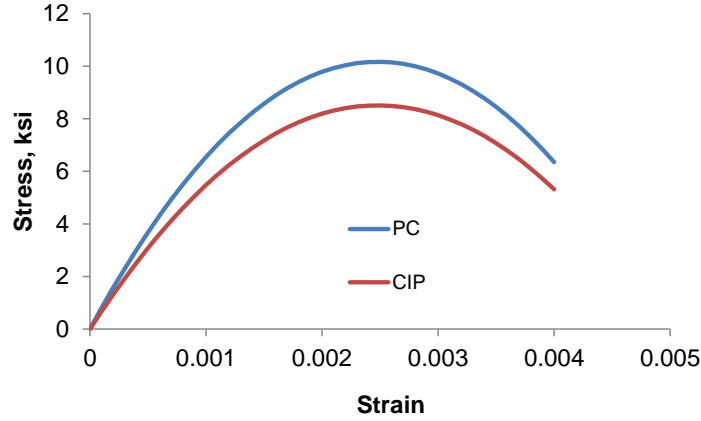


Figure 46. Stress-Strain Relationship for Concrete

$$f_{ps} = \begin{cases} E_{ps} \varepsilon_{ps} & \text{if } \varepsilon_{ps} \leq 0.0084 \\ 240 + 1515(\varepsilon_{ps} - 0.0084) & \text{if } 0.0084 \leq \varepsilon_{ps} \leq 0.015 \\ 250 + 444(\varepsilon_{ps} - 0.015) & \text{otherwise} \end{cases} \quad (21)$$

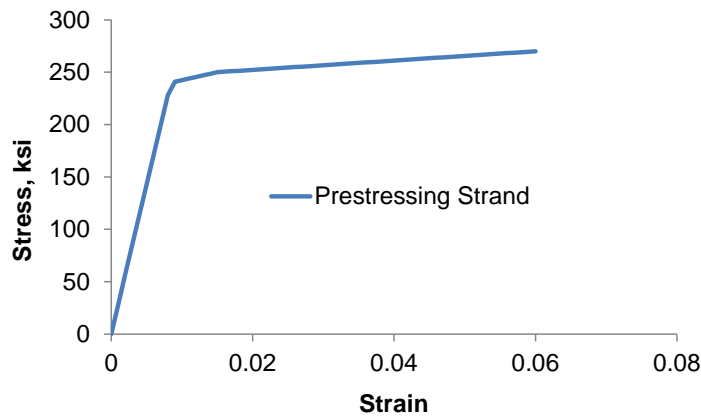


Figure 47. Stress-Strain Relationship for Prestressing Strand

Moment-Curvature Relationship

To obtain the anticipated full load versus mid-span deflection curve for the simply supported composite beam, a moment-curvature relationship had to be developed for any given cross section of the beam. Because the system consists of a pre-tensioned precast beam with straight strands and a cast-in-place topping, the moment-curvature relationship was constant throughout the span. After the moment-curvature relationship is defined, this information can be used to relate the moment diagram in the simply supported beam to a curvature diagram, which can then be used to calculate deflections at desired locations along the span.

The moment-curvature relationship up until the first crack was calculated using principles from linear-elastic mechanics of materials. For the non-composite section, strain profiles along the depth of the section were obtained by first calculating the stresses at the extreme fibers (Equation 22) and then dividing them by the modulus of elasticity of the precast beam (Equation 23). Curvatures were calculated based on the slope of the strain diagram (Equation 24) and

moments were calculated using statics (Equation 25). For the composite section, additional moments and curvatures up to first crack were calculated by using the section properties of the composite section (Equations 26 through 30).

Non-composite Section:

$$\sigma = \mp \frac{P_e}{A_{pc}} \mp \frac{P_e e y}{I_{pc}} \mp \frac{(M_{invT} + M_{cip}) 12 y}{I_{pc}} \quad (22)$$

$$\varepsilon = \frac{\sigma}{E} \quad (23)$$

$$\phi_{noncomposite} = \frac{\varepsilon_{bottom} - \varepsilon_{top}}{h_{pc}} \quad (24)$$

$$M_{noncomposite} = M_{invT} + M_{cip} \quad (25)$$

Composite Section:

$$M_{cracking} = \frac{\frac{1}{12} \left[f_r + \frac{P_e}{A_{pc}} + \frac{P_e e y_{botcomp}}{I_{pc}} - \frac{(M_{invT} + M_{cip}) 12 y_{botcomp}}{I_{pc}} \right] I_c}{y_{botcomp}} \quad (26)$$

$$\Delta \varepsilon = \mp \frac{M_{cracking} 12 y}{I_c E_{pc}} \quad (27)$$

$$\Delta \phi = \frac{\Delta \varepsilon_{bot} - \Delta \varepsilon_{top}}{h_{pc}} \quad (28)$$

$$M_{composite} = M_{noncomposite} + M_{cracking} \quad (29)$$

$$\phi = \phi_{noncomposite} + \Delta \phi \quad (30)$$

The cracking moment induced by actuator load was calculated by assuming a modulus of rupture equal to $7.5\sqrt{f'c}$. Total curvatures in the composite system up until the first crack were calculated simply by adding the additional curvatures due to loads in the composite system to the already calculated ones on the precast beam. Total moments were calculated using statics.

The slope of the moment-curvature curve defines the flexural stiffness of the precast before it was made composite and that of the composite system after the cast-in-place topping was placed. The difference in these slopes is illustrated in Figure 48.

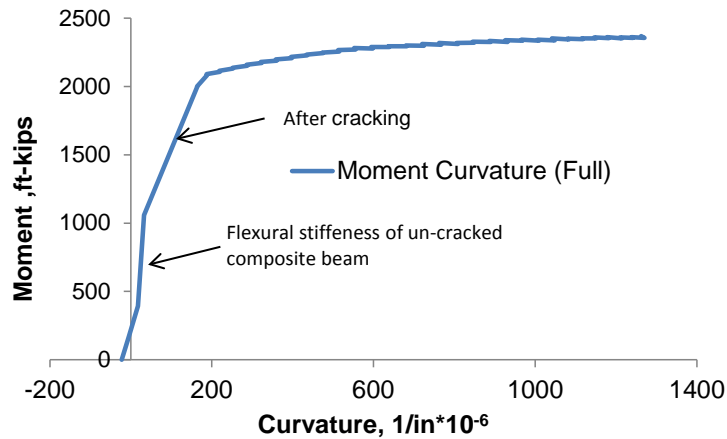


Figure 48. Full Moment-Curvature Relationship

An algorithm was used to obtain the moment-curvature relationship in the composite section after cracking. This algorithm is described in Menkulasi (2014) and consists of incrementally increasing the strain in the top of the cast-in-place concrete and finding the corresponding depth of the neutral axis. The strain in the top of the cast-in-place concrete and the depth to the neutral axis are used to calculate strain and stress profiles in the composite section. Compressive stress profiles in concrete are integrated to calculate internal compressive forces and the tensile stress in the steel is used to calculate the internal tension force. After internal equilibrium is satisfied, the internal moment, curvatures and the depth to the neutral axis are reported. Nilson (1987) states that the relatively small strain discontinuity at the interface between precast and cast-in-place concrete that results from prior bending of the non-composite precast section can be ignored without serious error at the overload stage. Because the strain range covered in this algorithm is relatively large, the strain discontinuity at the interface was ignored. However, the discontinuity of the concrete stress profiles at the interface of the two components was taken into account for cases when the neutral axis falls below the thinnest portion of the cast-in-place concrete topping.

Because the data from the test include the superimposed load (actuator load) versus the corresponding mid-span deflection, the full moment-curvature relationship (Figure 48) is adjusted to reflect just the superimposed moment and the corresponding curvature (Figure 49). This information is then used to construct a curvature diagram based on the moment in the composite beam caused by the actuator load (Figure 50). Deflection at mid-span of the beam is then calculated by multiplying the individual areas in the curvature diagram by the distance between their centroids and the support (Equation 31).

$$\Delta_{midspan} = \sum_{i=1}^n A_i y_i \tag{31}$$

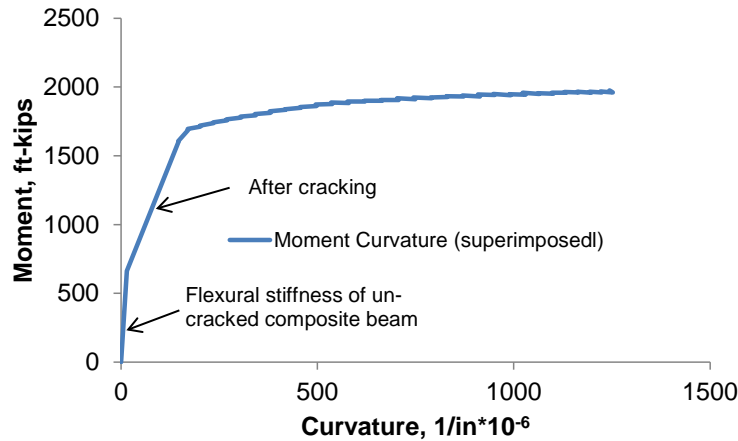


Figure 49. Moment-Curvature Relationship for Superimposed Loads

Experimental Results

Test 1 – Simulation of Service Level Design Moment

The purpose of the first test was to load the composite beam to simulate the service level design positive moment. The actuator load required to cause this moment was estimated to be 40

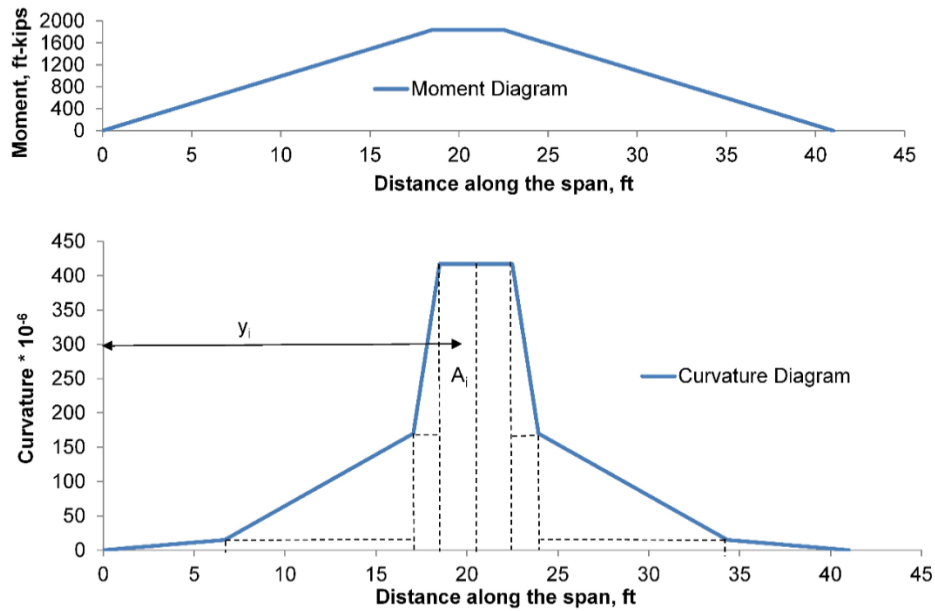


Figure 50. Moment and Curvature Diagram

kips ($P_{service}$). No cracking was observed in the precast beam during this test, which was consistent with the design requirements for a fully prestressed member. Figure 51 shows a comparison of the estimated and tested load versus mid-span deflection curves for the first test. As can be seen, the curves are almost identical, which provides evidence that full composite action was maintained up until the service level moment. Also, a comparison of the load versus quarter-span deflection curves is presented in Figure 52. These curves are also almost identical despite the fact that one half of the span contained extended stirrups whereas the other half did not. This shows that the extended stirrups are not required to ensure composite action up until the service level design positive moment. In addition, an examination of the typical load versus slip relationship at both ends of the beam, with and without extended stirrups, suggests that there is no slip at either end (Figure 53 and Figure 54), and confirms the assumption for full composite action.

Test 2 – Simulation of Strength Level Design Shear (V_u)

The purpose of the second test was to simulate strength level design vertical shear on the portion of the beam without the extended stirrups. The actuator load required to simulate this condition was estimated to be 118 kips (P_{Vu}). Figure 55 and Figure 56 reveal that there was no slip at either end of the beam under this load arrangement, which confirmed the hypothesis that the composite beam can resist the strength level design shear force without incurring any slip, even with no extended stirrups. The maximum horizontal shear stress computed using Equation 15 was 99 psi. This observation leads to the conclusion that the design for horizontal shear of composite bridge systems consisting of adjacent precast inverted T-beams with tapered webs and cast-in-place topping can be confidently based on a cohesion factor equal to at least 99 psi.

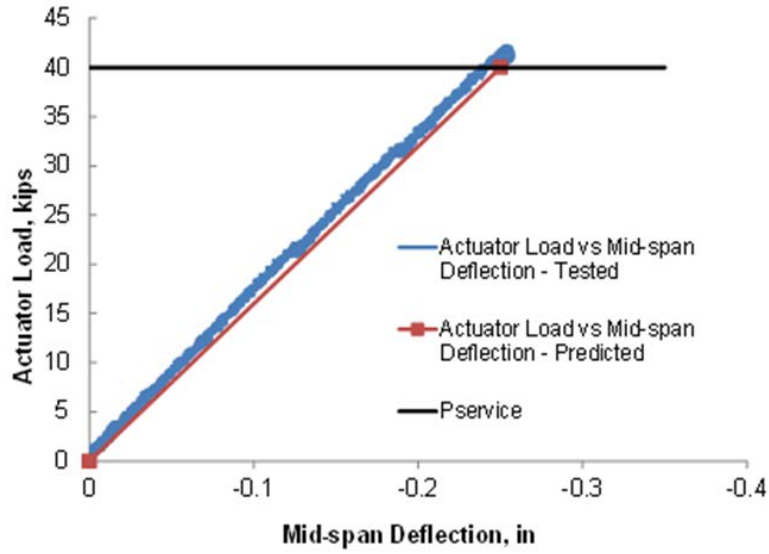


Figure 51. Comparison of Predicted and Experimental Load vs. Mid-Span Deflection Curves (Up to $P_{service}$)

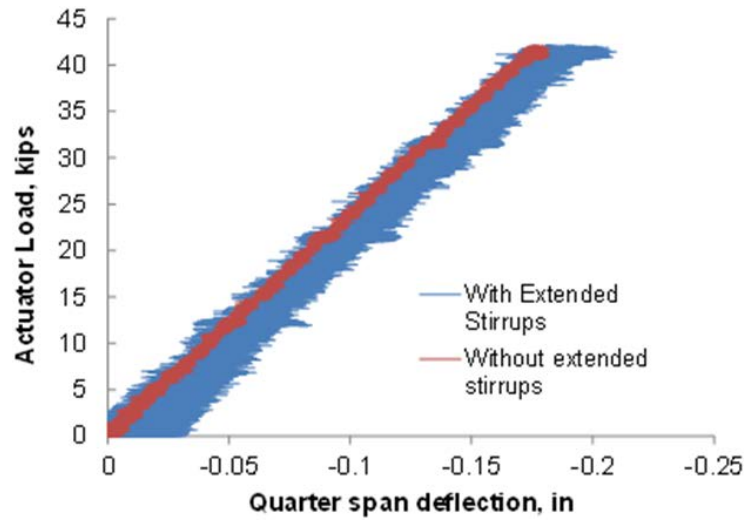


Figure 52. Comparison of Load Quarter-Span Deflection Curves (Up to $P_{service}$)

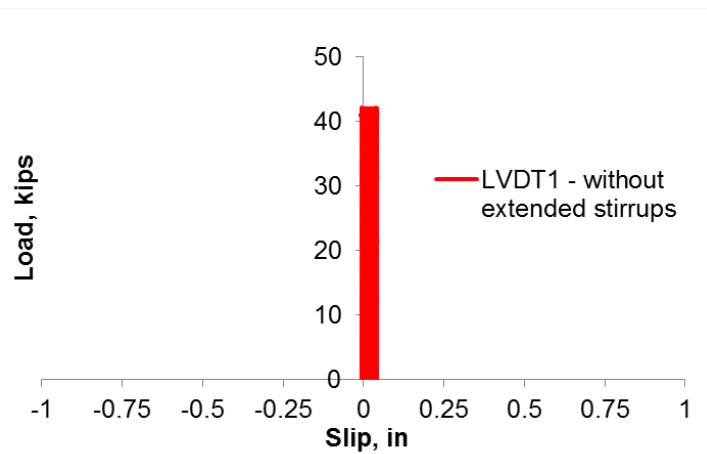


Figure 53. Typical Load vs. Slip Relationship, Without Extended Stirrups (Up to $P_{service}$)

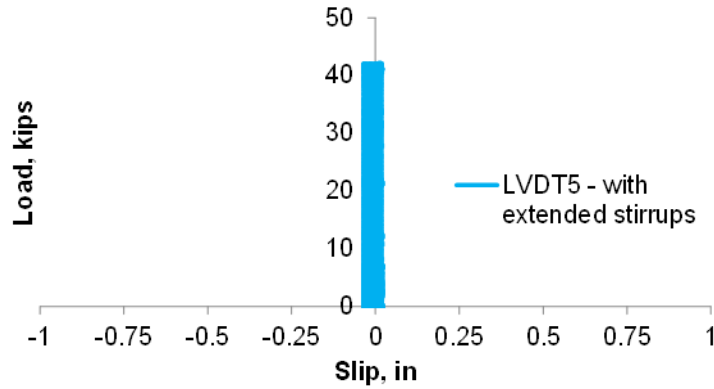


Figure 54. Typical Load vs. Slip Relationship, With Extended Stirrups (Up to $P_{service}$)

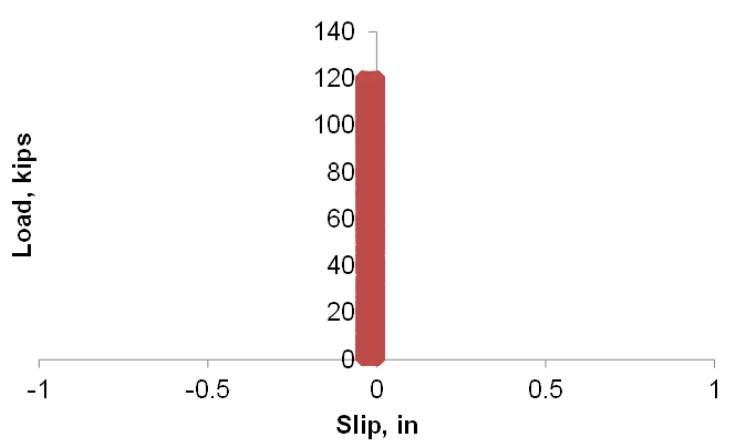


Figure 55. Typical Load vs. Slip Relationship, Without Extended Stirrups (Up to P_{vu})

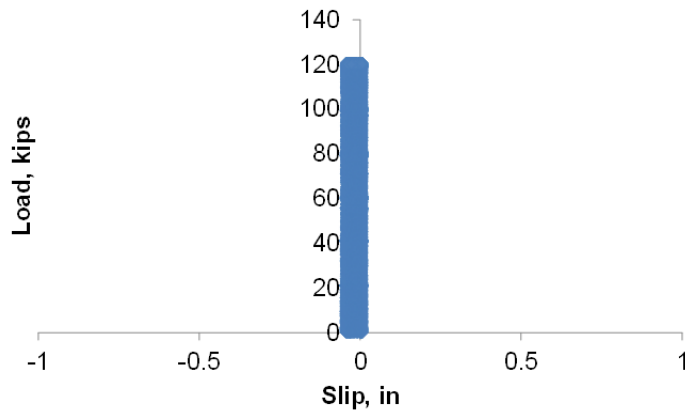


Figure 56. Typical Load vs. Slip Relationship, With Extended Stirrups (Up to P_{vu})

Test 3 – Simulation of Nominal Moment Capacity (M_n)

The purpose of the third test was to simulate moments in the composite section that were equal to the strength level design positive moment and the nominal moment capacity of the composite section. The actuator loads required to simulate the strength level design positive moment and nominal moment capacity were 76 kips (P_{Mu}) and 200 kips (P_{Mn}), respectively. The capacity of the actuator was 220 kips. The composite beam was loaded until the capacity of the

actuator was met. Figure 57 shows a comparison between the estimated actuator load versus mid-span deflection curve and the experimentally obtained curve. It can be seen that the two curves are similar, with the experimental curve exhibiting slightly higher strength and stiffness than estimated. A part of the small difference between the experimental and predicted curve can be attributed to the fact that tension stiffening was ignored in the prediction method used herein. Figure 58 shows a comparison of the actuator load versus quarter-span deflection relationship. As can be seen, the two curves are identical, which suggests that the behavior of the half of the span without extended stirrups is identical to that of the other half of the span that features extended stirrups. This observation confirms the hypothesis that the extended stirrups are not required to maintain full composite action up to the development of the nominal moment capacity of the composite beam.

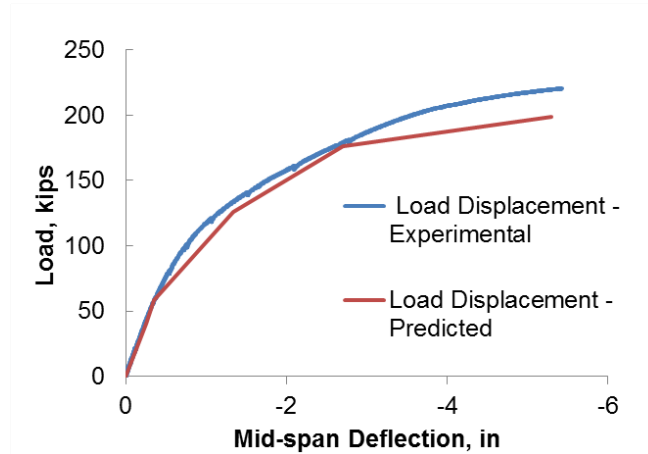


Figure 57. Comparison of Predicted and Experimental Load vs. Mid-Span Deflection Curves (Full Curve)

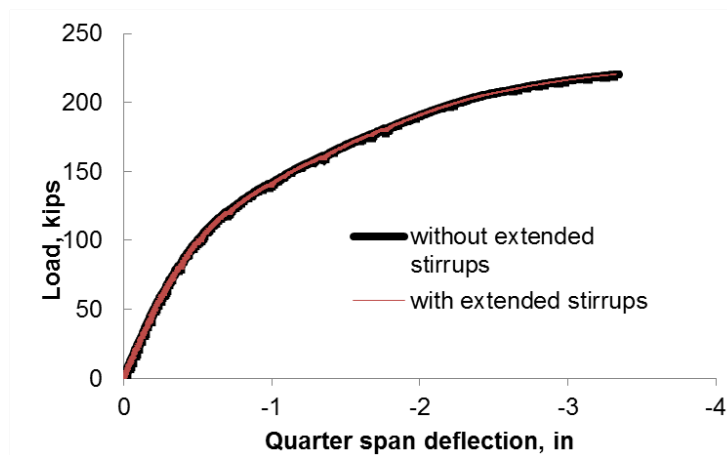


Figure 58. Comparison of Load Quarter-Span Deflection Curves (Up to P_{mn})

Figure 59 and Figure 60 show that there is no slip at either end of the composite beam, an observation that provides additional evidence about the ability of the composite beam to develop its nominal moment capacity without incurring any slip. The maximum vertical shear force at the critical section when the actuator load reached 220 kips was equal to 147 kips, which was larger than the strength level design vertical shear forces at the critical section (138 kips). Because the failure mode of the composite beam under the loading arrangement illustrated in Test 3 was of interest, the 220-kip actuator was replaced with a 400-kip actuator, and the

composite beam was loaded to failure. The composite beam failed in flexure at an actuator load of 272 kips. The corresponding vertical shear force at the critical section was 173 kips including the self-weight of the composite beam. The horizontal shear stresses computed using Equation 15, 17, and 18 in the previously investigated planes are provided in Table 17. The maximum computed horizontal shear stress was 124 psi in Plane 1 and was based on Equation 15. Although the composite beam at failure exhibited significant flexural cracking, the regions near the support, with the highest vertical shear, did not exhibit cracking. Accordingly, the utilization of Equation 15 for these regions is valid. In addition, the horizontal shear stresses computed using Equation 17 in Planes 1 and 2 were 120 psi. As expected, horizontal shear stresses computed using Equation 18 were lower and were equal to 110 psi for Planes 1 and 2 and 95 psi for Plane 3. Because Equation 18 is provided in AASHTO as a reasonable approximation of the horizontal shear stress, these results suggest that the design for horizontal shear of adjacent precast inverted T-beams with tapered webs and cast-in-place topping can be confidently based on the following cohesion and friction factors: $c = 120$; $\mu = 1.0$; $K_1 = 0.2$; and $K_2 = 0.8$.

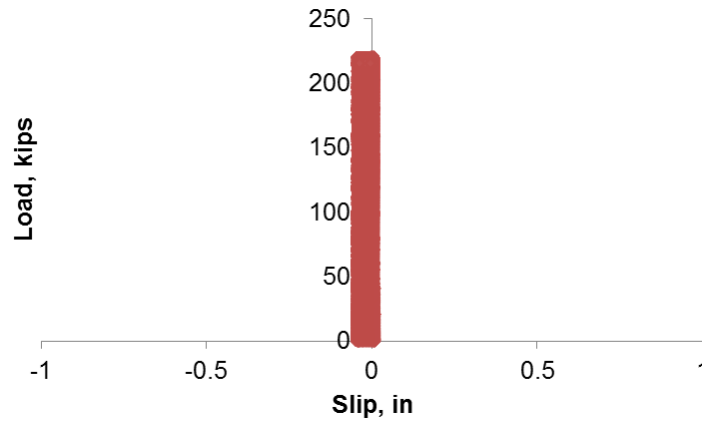


Figure 59. Typical Load vs. Slip Relationship, Without Extended Stirrups (Up to P_{Mn})

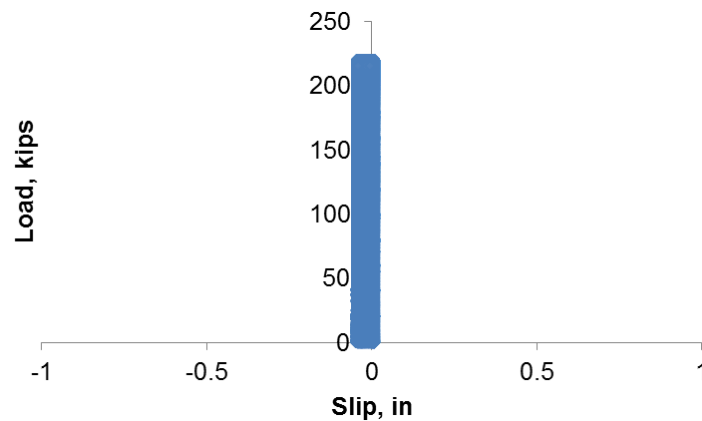


Figure 60. Typical Load vs. Slip Relationship, With Extended Stirrups (Up to P_{Mn})

Because of the flexural failure mode, the 120-psi horizontal shear stress representing the recommended cohesion factor does not constitute the maximum horizontal shear stress that can be developed in the composite inverted T-beam system described herein. The flexural failure of

the composite beam prevented it from achieving higher horizontal shear stresses at the interfaces, such as those achieved by French et al. (2011) (135 psi) in their experiments.

Table 17. Horizontal Shear Stress (Based on Actuator Load That Caused Failure)

Eq.	Horizontal Shear Stress, psi		
	Plane 1	Plane 2	Plane 3
15	124	82	Varies
17	120	120	NA
18	110	110	95

NA = not applicable.

CONCLUSIONS

Investigation of Cross-Sectional Shape and Transverse Connection

- *The inverted T-beam is a useful and promising system for short-to-medium-span bridges that delivers the advantages of seamless, cast-in-place, concrete construction while eliminating the need for installing formwork.* It addresses the reflective cracking problem by providing a thicker cast-in-place topping over the joint between the precast members.
- *Transverse bottom reinforcement can be sized using allowable stress design principles by ignoring any contribution from concrete in tension.* The transverse reinforcement sized in this manner will act as transverse load distribution reinforcement and reflective crack control reinforcement for details that are similar to the ones tested in Specimen Nos. 2 through 7.
- *In lieu of performing such an analysis, if the ratio of the thickness of the cast-in-place topping over the joint to the thickness of the precast flange is similar to the one used in the US 360 Bridge described in this report, then the transverse bottom reinforcement (in the cast-in-place topping and in the precast beam) can be sized based on Equation 3.* The areas of transverse steel calculated based on the transverse live load moment obtained from finite element analyses and Equation 3 were similar for the US 360 Bridge.
- *Tapering the webs of the precast inverted T-beams provides a higher resistance against normal tensile stresses in the transverse direction.* The inverted T-beam system had improved behavior compared to the Poutre-Dalle system with vertical webs.
- *Roughening the surfaces of the precast inverted T-beams that will be in contact with the cast-in-place topping results in the composite system emulating monolithic action and provides the necessary integrity to prevent cracking due to service level loads as a result of plate bending in the transverse direction.* All eight specimens, which featured combinations of two cross-sectional shapes and three connections, performed well and similarly at service load levels.
- *The detail with the tapered webs and no mechanical connection is the least expensive and the easiest to fabricate.* This detail is ideal because there is no reinforcing steel protruding from

the sides of the webs, which presents a forming challenge for the precaster. Furthermore, the absence of a mechanical connection between the precast members reduces installation time in the field.

Deck Mixture Design Optimization Study

- *Concrete mixtures for the cast-in-place deck that possess low shrinkage and high creep properties can reduce the likelihood of excessive cracking.* Low free shrinkage reduces the tensile stresses that can develop when the concrete is restrained by differential shrinkage and high creep helps relax any tensile stresses that may develop.
- *The short-term properties that help reduce the extent of cracking due to differential shrinkage include high tensile strength and low modulus of elasticity.*
- *It is difficult to find a concrete mixture that embodies all the aforementioned long-term and short-term properties; the mixture with the lowest shrinkage is desirable because the free shrinkage of the deck serves as a catalyst for the creation of tensile stresses in the cast-in-place topping.*
- *The mixture with normal-weight coarse aggregates and saturated lightweight fine aggregates (NWC-SLWF) exhibited the lowest shrinkage strain, based on drying shrinkage strains recorded in the shrinkage prisms of the seven deck mixtures investigated.*
- *The mixture with normal-weight coarse aggregates and saturated lightweight fine aggregates (NWC-SLWF) also exhibited the highest creep coefficient, based on data obtained from the creep test. Note that the tests performed on the deck mixtures described in this investigation were performed only on one batch for each mixture because repeatability and consistency of the results obtained from each mixture were outside the scope of this study. Although the NWC-SLWF mixture performed well in terms of shrinkage and creep, the permeability of the hardened concrete may be unacceptably high because there is no supplemental cementitious material in the mixture.*

Composite Action Study

- *Full composite behavior in the uniquely shaped inverted-T composite system is assured not only at service and strength level design loads, but also up to flexural failure, based on the full-scale test.*
- *Extending stirrups from the precast into the cast-in-place topping may not be necessary; adequate horizontal shear resistance can be provided solely by the natural adhesion and friction along the interface to develop the nominal moment capacity of the composite section.* The composite inverted T-beam bridge system with tapered webs and cast-in-place topping features a broad contact surface between the precast and cast-in-place components. The presence of extended stirrups in one half of the span did not result in any differences in behavior between the two halves of the span.

- *Roughening the tapered webs and the tops of the precast flanges in the longitudinal direction while providing a transverse rake finish only at the top of the precast web appears to provide adequate horizontal shear resistance in the longitudinal direction to resist at least a horizontal shear stress of 120 psi without the presence of extended stirrups.* The minimum reinforcement requirements for cases in which the horizontal shear stress is smaller than 120 psi and the precast surfaces are roughened as described above can be waived for composite bridges consisting of adjacent precast inverted T-beams with tapered webs and cast-in-place topping.
- *Equation 17, as provided in AASHTO (2013), provides a reasonable approximation of the horizontal shear stress. Results suggest that the design for horizontal shear of adjacent precast inverted T-beams with tapered webs and cast-in-place topping can be confidently based on the following cohesion and friction factors: $c=120$ psi, $\mu=1.0$, $K1=0.2$, $K2=0.8$.* The composite bridge system in this study and used in the construction of the US 360 Bridge was able to develop a horizontal shear stress equal to at least 120 psi without the presence of extended stirrups. The failure mode of the composite section was a flexural failure. Because of the flexural failure mode, the 120 psi horizontal shear stress representing the recommended cohesion factor does not constitute the maximum horizontal shear stress that can be developed in the composite inverted T-beam system described herein. The flexural failure of the composite beam prevented it from achieving higher horizontal shear stresses at the interfaces such as those achieved by French et al. (2011) (135 psi) in their experiments. The recommended cohesion and friction factors are also notably conservative compared to the AASHTO factors for light weight concrete placed monolithically, or nonmonolithically, against a clean concrete girder surface that is free of laitance and is roughened to an amplitude of 0.25 in (AASHTO, 2013). These recommended values may increase with additional test results.

RECOMMENDATIONS

1. *VDOT's Structure and Bridge Division should adopt an inverted T-beam cross-section with tapered webs, similar to that used in this project, as a standard design for short-to-medium-span prestressed concrete adjacent member bridges.*
2. *VDOT's Structure and Bridge Division should consider using a welded transverse connection, similar to Test Specimen No. 3, on bridges with high volumes of truck traffic.*
3. *VDOT's Structure and Bridge Division should use a non-contact lap splice transverse connection, similar to Test Specimens No. 5 and No. 6, on bridges with low volumes of truck traffic.*
4. *VDOT's Structure and Bridge Division should determine the quantity of transverse reinforcement for load distribution based on the analytical method described in this report or, if the bridge is of similar configuration to the US 360 Bridge, based on Equation 3.*

5. *VDOT's Structure and Bridge Division should specify a concrete topping mixture with a low shrinkage strain and a high creep coefficient. A mixture similar to the NWC-SLWF design used in this study will satisfy this requirement; however, the mix design should incorporate a supplemental cementitious material to decrease permeability. Mindess et al. (2003) stated that "it has been widely observed that the addition of supplementary cementitious materials, especially silica fume, results in a significant decrease in permeability." Cousins et al. (2013) confirmed those observations in NCHRP Report 733.*
6. *VDOT's Structure and Bridge Division should specify that the top surface of the bottom flanges and the tapered sides of the web have a roughened surface with the pattern running in the longitudinal direction of the bridge. The top surface of the web should be roughened with the pattern running in the transverse direction. A 1/4-in amplitude in surface roughness can be achieved by raking, forming, surface retarder, etc.*
7. *VDOT's Structure and Bridge Division should design the inverted T-beam system for horizontal shear using the methods prescribed in the AASHTO LRFD Bridge Design Specifications, using the following cohesion and friction factors: $c = 120$ psi, $\mu = 1.0$, $K1 = 0.2$, and $K2 = 0.8$.*
8. *The Virginia Transportation Research Council should support additional research to determine if the non-contact lap splice connection can be used on bridges with high volumes of truck traffic. This testing should use sub-assembly test specimens subjected to cyclic loads. Additional topping mixtures with saturated lightweight fines and a supplemental cementitious material should be investigated.*

BENEFITS AND IMPLEMENTATION

Benefits

The benefit of the inverted T-beam system is improved durability compared to traditional adjacent member systems such as box beams or voided slabs. The cast-in-place topping over the joint between the members is deeper and more heavily reinforced than in the traditional systems. Therefore, if a crack does develop at the joint at the bottom of the cross section, it is far less likely to propagate to the surface and result in a full-depth crack. Full-depth cracks in traditional adjacent member bridges allow water and deicing salts a direct path to the underside of the bridge, where they can cause early initiation of corrosion in the prestressed beams. The inverted T-beam system should be much more durable.

The benefits of implementing the study recommendations would be an improved cross-sectional shape, which should reduce the likelihood of reflective cracking over the tops of the webs, and new connection details, which should improve constructability. The research into topping mixtures resulted in one viable mix design, which was used in the Route 360 Bridge, and several other mixtures that showed promise but need further refinement. The composite action testing revealed that horizontal shear connectors are not needed, which will improve the economy and constructability of the system.

Implementation

The inverted T-beam system has already been used in the Route 360 Bridge and the Towlston Road Bridge. This study provided the foundation for the development of VDOT standards for this type of system.

With regard to Recommendations 1 through 7, VDOT's State Structure and Bridge Engineer and his staff will oversee their implementation in terms of the development of standard design details and any associated special provisions (with assistance from Virginia Tech) for incorporation into VDOT's *Manual of the Structure and Bridge Division* for span lengths of 20 ft to at least 45 ft. The Appendix provides a basic concrete mix design that can be used for the topping. These standards will be completed by March 2018. However, additional investigative effort may be required to refine designs for exterior beams to support barriers and to determine limitations on the maximum viable length of inverted-T spans.

With regard to Recommendation 8, a follow-on study has already been initiated, with an anticipated completion date of January 2019.

ACKNOWLEDGMENTS

The authors gratefully acknowledge the guidance and assistance of Michael Brown, formerly of the Virginia Transportation Research Council; Bernie Kassner of the Virginia Transportation Research Council; and Chris Lowe and Andy Zickler of VDOT's Structure and Bridge Division. The assistance of Brett Farmer, Carrie Field, Kedar Halbe, Dennis Huffman, Matt Mercer, David Mokarem, and Doug Nelson in the field and at the Murray Structural Engineering Laboratory at Virginia Tech is gratefully acknowledged. The opinions expressed in this report are those of the authors and not necessarily those of the sponsoring agencies.

REFERENCES

- ABAQUS. *User's Manual Version 6.11-2*. Dassault Systemes Simulia Corp., Johnston, RI, 2012.
- ACI Committee 209. *Guide for Modeling and Calculating Shrinkage and Creep in Hardened Concrete*. American Concrete Institute, Farmington Hills, MI, 2008.
- ACI Committee 318. *Building Code Requirements for Structural Concrete and Commentary*. American Concrete Institute, Farmington Hills, MI, 2014.
- American Association of State Highway and Transportation Officials. *AASHTO LRFD Bridge Design Specifications, Sixth Edition*. Washington, DC, 2013.
- ASTM International. *ASTM C39: Test Method for Compressive Strength of Cylindrical Concrete Specimens*. West Conshohocken, PA, 2010a.

- ASTM International. *ASTM C157: Standard Test Method for Length Change of Hardened Hydraulic-Cement Mortar and Concrete*. West Conshohocken, PA, 2010b.
- ASTM International. *ASTM C469: Standard Test Method for Static Modulus of Elasticity and Poisson's Ratio of Concrete in Compression*. West Conshohocken, PA, 2010c.
- ASTM International. *ASTM C496: Standard Test Method for Splitting Tensile Strength of Cylindrical Concrete Specimens*. West Conshohocken, PA, 2010d.
- ASTM International. *ASTM C512: Standard Test Method for Creep of Concrete in Compression*. West Conshohocken, PA, 2010e.
- Barker, R.M. and Puckett, J.A. *Design of Highway Bridges—An LRFD Approach*, Second Edition. John Wiley & Sons, Inc., Hoboken, NJ, 2007.
- Bazant, Z.P. Prediction of Concrete Creep Effects Using the Age Adjusted Effective Modulus Method. *ACI Journal*, Vol. 69, No. 4, 1972, pp. 212-217.
- Bazant, Z.P. Statistical Extrapolation of Shrinkage Data – Part I: Regression. *ACI Materials Journal*, Vol. 84, No. 1, 1987, pp. 20-34.
- Bell, C., Shield, C.K., and French, C.W. *Application of Precast Decks and Other Elements to Bridge Structures*. MN/RC 2006-37. Minnesota Department of Transportation, Saint Paul, 2006.
- Cousins, T., Roberts-Wollmann, C., and Brown, M.C. *NCHRP Report 733: High-Performance/High-Strength Lightweight Concrete for Bridge Girders and Decks*. Transportation Research Board, Washington, DC, 2013.
- Dimaculangan, C.M. and Lesch, T. Minnesota's Precast Composite Slab Span System. *Aspire*, Summer 2010.
- French, C.W., Shield, C.K., Klasesus, D., Smith, M., Eriksson, W., Ma, J.Z., Zhu, P., Lewis, S., and Chapman, C.E. *Cast-in-Place Concrete Connections for Precast Deck Systems*. NCHRP Web-Only Document 173. Transportation Research Board, Washington, DC, January 2011. <http://www.trb.org/Publications/Blurbs/164971.aspx>. Accessed Oct. 12, 2017.
- Hagen, K., Ellis, S., Fishbein, J., Molnau, K., Wolhowe, E., and Dorgan, D. Development and Construction of a Precast Inverted T System for Expediting Minnesota Slab Span Bridge Projects. In *Proceedings of the PCI 2005 National Bridge Conference*, Palm Springs, CA, October 16-19, 2005.
- Halverson, M., French, C., and Shield, C. *Full-Depth Precast Concrete Bridge Deck System: Phase II*. MN/RC 2012-30. Minnesota Department of Transportation, Saint Paul, 2012.

- Hanson, N.W. *Precast-Prestressed Concrete Bridges 2: Horizontal Shear Connections*. Portland Cement Association, Research and Development Laboratories, Skokie, IL, 1960.
- Hill, J.C., and Lowe, C.M. *Route 360 Over Chickahominy River Bridge Replacements Hanover/Henrico Counties, Richmond District State Project 0360-964-120, B601, B606, B607 & B608 - Federal Structure Identification Numbers 9469, 10014, 10015, 10016 UPC Number 17959 - Preliminary Structure Report, Plans and Estimates*. Virginia Department of Transportation, Central Office Structure & Bridge Division, Richmond, May 3, 2010.
- Hognestad, E. *A Study of Combined Bending and Axial Load in Reinforced Concrete Members*. Bulletin 399. University of Illinois Engineering Experiment Station, Urbana, IL, 1951.
- Loov, R.E., and Patnaik, A.K. Horizontal shear strength of composite concrete beams with a rough interface. *PCI Journal*, Vol. 39, No. 1, 1994, pp. 48-68.
- Menkulasi, F. *The Development of a Composite Concrete Bridge System for Short-to-Medium-Span Bridges*, Ph.D. dissertation, Virginia Tech, Blacksburg, 2014.
- Mindess, S., Young, J.F., and Darwin, D. *Concrete*, Second Edition. Pearson, Upper Saddle River, NJ, 2003.
- Nilson, A.H. *Design of Prestressed Concrete*. John Wiley & Sons, New York, 1987.
- Ralls, M.L., Tang, B., Bhide, S., Brecto, B., Calvert, E., Capers, H., Dorgan, D., Matsumoto, E., Napier, C., Nickas, W., and Russell, H. *Prefabricated Bridge Elements and Systems in Japan and Europe*. FHWA-PL-05-003. Federal Highway Administration, Washington, DC, 2005.
- Saemann, J.C., and Washa, G.W. Horizontal Shear Connections Between Precast Beams and Cast-in-Place Slabs. *ACI Journal Proceedings*, Vol. 61, No. 11, 1964.
- Smith, M., Eriksson, W., Shield, C., and French, C. Field and Laboratory Study of the Mn/DOT Precast Slab Span System. In *Proceedings of the 2007 Mid-Continent Transportation Research Symposium*, Ames, Iowa, 2007.
- Smith, M.J., Eriksson, W.D., Shield, C.K., and French, C.W. *Monitoring and Analysis of Mn/DOT Precast Composite Slab Span System (PCSSS)*. MN/RC 2008-41. Minnesota Department of Transportation, Saint Paul, 2008.

APPENDIX

MIX DESIGN FOR THE TOPPING CONCRETE USED IN THE US 360 BRIDGE (B607, VA STRUCTURE NO. 0431018)

Constituent	Quantity ^a	Source
Type II Cement	476 lb	Lehigh
Fly Ash	159 lb	SEFA
No. 57 Course Aggregate	1720 lb	Luck Stone
Fine Aggregate	1151 lb	Brett Aggregate
Water	286 lb	Municipality
Air Entrainment Admixture	1.2 oz	Sika AEA-15
Retarder	As needed	Sika Plastiment
Water Reducer	19.05 oz	Sika Plastocrete 161
High Range Water Reducer	12.7 oz	Sika ViscoCrete 2100

^aAll quantities are per cubic yard of concrete.